Year : 2011

The biology of cancer stem cells. Part 1: Nuclear translocation of CD44. Part 2: Imp2 in glioblastoma cancer stem cells

Michalina Janiszewska

UNIL | Université de Lausanne
Faculté de biologie et de médecine

Département de Pathologie

THE BIOLOGY OF CANCER STEM CELLS
PART 1: NUCLEAR TRANSLOCATION OF CD44
PART 2: IMP2 IN GLIOBLASTOMA CANCER STEM CELLS

Thèse de doctorat ès sciences de la vie (PhD)

présentée à la

Faculté de Biologie et de Médecine
de l'Université de Lausanne

par

Michalina JANISZEWSKA

Master de l'Université de Wroclaw, Pologne

Jury

Prof. Alfio Marazzi, Président
Prof. Ivan Stamenkovic, Directeur de thèse
Prof. Douglas Hanahan, expert
Prof. Pedro Romero, expert

Lausanne 2011

UNIL | Université de Lausanne
Faculté de biologie
et de médecine

Ecole Doctorale

Doctorat ès sciences de la vie

Imprimatur

Vu le rapport présenté par le jury d'examen, composé de

Président	Monsieur	Prof. Alfio **Marazzi**
Directeur de thèse	Monsieur	Prof. Ivan **Stamenkovic**
Experts	Monsieur	Prof. Pedro **Romero**
	Monsieur	Prof. Douglas **Hanahan**

le Conseil de Faculté autorise l'impression de la thèse de

Madame Michalina Janiszewska

Master of the University of Wroclaw, Pologne

intitulée

The biology of cancer stem cells
Part 1: nuclear translocation of CD44
Part 2: IMP2 in glioblatoma cancer stem cells

Lausanne, le 16 septembre 2011

pour Le Doyen
de la Faculté de Biologie et de Médecine

Prof. Alfio Marazzi

Table of contents

Summary

Cancer stem cells (CSC) are poorly differentiated, slowly proliferating cells, with high tumorigenic potential. Some of these cells, as it has been shown in leukemia, evade chemo- and radiotherapy and recapitulate the tumor composed of CSC and their highly proliferative progeny. Therefore, understanding the molecular biology of those cells is crucial for improvement of currently used anti-cancer therapies.

This work is composed of two CSC-related projects. The first deals with CD44, a frequently used marker of CSC; the second involves Imp2 and its role in CSC bioenergetics.

PART 1. CD44 is a multifunctional transmembrane protein involved in migration, homing, adhesion, proliferation and survival. It is overexpressed in many cancers and its levels are correlated with poor prognosis. CD44 is also highly expressed by CSC and in many malignancies it is used for CSC isolation.

In the present work full-lenght CD44 nuclear localization was studied, including the mechanism of nuclear translocation and its functional role in the nucleus. Full-length CD44 can be found in nuclei of various cell types, regardless of their tumorigenic potential. For nuclear localization, CD44 needs to be first inserted into the cell membrane, from which it is transported via the endocytic pathway. Upon binding to transportin1 it is translocated to the nucleus. The nuclear localization signal recognized by transportin1 has been determined as the first 20 amino acids of the membrane proximal intracellular domain. Nuclear export of CD44 is facilitated by exportin Crm1. Investigation of the function of nuclear CD44 revealed its implication in *de novo* RNA synthesis.

PART 2. Glioblastoma multiforme is the most aggressive and most frequent brain malignancy. It was one of the first solid tumors from which CSC have been isolated. Based on the similarity between GBM CSC and normal stem cells expression of an oncofetal mRNA binding protein Imp2 has been investigated.

Imp2 is absent in normal brain as well as in low grade gliomas, but is expressed in over 75% GBM cases and its expression is higher in CSC compared to their more differentiated counterparts. Analysis of mRNA transcripts bound by Imp2 and its protein interactors revealed that in GBM CSC Imp2 may be implicated in mitochondrial metabolism. Indeed, shRNA mediated silencing of protein expression led to decreased mitochondrial activity, decreased oxygen consumption and decreased activity of respiratory chain protein complex I. Moreover, lack of Imp2 severely affected self-renewal and tumorigenicity of GBM CSC. Experimental evidence suggest that GBM CSC depend on mitochondrial oxidative

phosphorylation as an energy producing pathway and that Imp2 is a novel regulator of this pathway.

Résumé

Les cellules cancéreuses souches sont des cellules peu différentiées, à proliferation lente et hautement tumorigénique. Ces cellules sont radio-chimio résistantes et sont capable reformer la tumeur dans sont intégralité, reproduisant l'hétérogénéité cellulaire présent dans la tumeur d'origine. Pour améliorer les therapies antitumorales actuelles il est crucial de comprendre les mécanismes moléculaires qui caractérisent cette sous-population de cellules hautement malignes.

Ce travail de thèse se compose de deux projets s'articulant autour du même axe :

Le CD44 est une protéine multifonctionnelle et transmembranaire très souvent utilisée comme marqueur de cellules souches tumorales dans différents cancers. Elle est impliquée dans la migration, l'adhésion, la prolifération et la survie des cellules. Lors de ce travail de recherche, nous nous sommes intéressés à la localisation cellulaire du CD44, ainsi qu'aux mécanismes permettant sa translocation nucléaire. En effet, bien que principalement décrit comme un récepteur de surface transmembranaire, le CD44 sous sa forme entière, non clivée en peptides, peut également être observé à l'intérieur du noyau de diverses cellules, quel que soit leur potentiel tumorigénique. Pour passer ainsi d'un compartiment cellulaire à un autre, le CD44 doit d'abord être inséré dans la membrane plasmique, d'où il est transporté par endocytose jusqu'à l'intérieur du cytoplasme. La transportin1 permet ensuite la translocation nucléaire du CD44 via une « séquence signal » contenue dans les 20 acides aminés du domaine cytoplasmique qui bordent la membrane. A l'inverse, le CD44 est exporté du noyau grâce à l'exportin Crm1. En plus des mécanismes décrits ci-dessus, cette étude a également mis en évidence l'implication du CD44 dans la synthèse des ARN, d'où sa présence dans le noyau.

Le glioblastome est la plus maligne et la plus fréquente des tumeurs cérébrales. Dans ce second projet de recherche, le rôle de IMP2 dans les cellules souches tumorales de glioblastomes a été étudié. La présence de cette protéine oncofoetale a d'abord été mise en évidence dans 75% des cas les plus agressifs des gliomes (grade IV, appelés glioblastomes), tandis qu'elle n'est pas exprimée dans les grades I à III de ces tumeurs, ni dans le cerveau sain. De plus, IMP2 est apparue comme étant davantage exprimée dans les cellules souches tumorales que dans les cellules déjà différenciées. La baisse de l'expression de IMP2 au moyen de shRNA a résulté en une diminution de l'activité mitochondriale, en une réduction de la consommation d'oxygène ainsi qu'en une baisse de l'activité du complexe respiratoire I.

L’inhibition de IMP2 a également affecté la capacité de renouvellement de la population des cellules souches tumorales ainsi que leur aptitude à former des tumeurs.

Lors de ce travail de thèse, une nouvelle fonction d’un marqueur de cellules souches tumorales a été mise en évidence, ainsi qu’un lien important entre la bioénergétique de ces cellules et l’expression d’une protéine oncofoetale.

General introduction

Cancer is a disease of abnormal cellular proliferation leading to tumor formation. Cells undergo malignant transformation as a result of various mutations, which allow them to evade regulatory mechanisms that constrain normal tissues from excessive proliferation. During tumor progression cancer cells acquire several biological features that change their physiology and sustain cancer growth – self-dependence on growth signaling, resistance to growth-inhibitory signals, escape from programmed cell death, unlimited replicative capability, activation of angiogenic signaling, tissue invasion and metastasis [1]. These cancer hallmarks are often underlined by genetic alterations in two classes of genes – oncogenes and tumor suppressor genes. Mutations in oncogenes, such as RAS and MYC, deregulate pathways leading to enhanced cell proliferation and distorted expression of tumor-suppressors, as p53 or Rb, provides a means to escape from proliferation control. Although it seems that all cancer types need to sustain growth and survival of tumor cells, various combinations of molecular dysfunctions can lead to the same outcome due to the complexity and redundancy of cellular signaling networks. This heterogeneity of molecular causes of malignant transformation in different tumors is one of the reasons for low efficiency of current therapies.

Although cancers can be characterized by distinct molecular features, their behavior, described as hallmarks of cancer, remains the same. Thus, the design of first cancer therapies focused on a feature common to most cancers – proliferation – and was directed to kill the rapidly dividing tumor cells. However, this approach was assuming homogeneity of a given tumor – equal proliferating capacity of all the cells within the tumor mass. As early as in the 1930s it had become clear, that tumors are heterogenous [2]. Cells within a tumor can differ in their morphology, but also in their proliferative capacity and the ability to recapitulate a tumor upon injection into immunocompromised animals [2, 3].

The heterogeneity of cancer cells within a tumor can be explained by one of the following models (Fig.1) [3]. The stochastic model assumes that cancer cells are biologically equal and that they are equally sensitive to intrinsic or extrinsic factors. Those factors, such as active cellular signaling pathways or signaling initiated by the tumor microenvironment, are unpredictable and they vary within a given tumor, creating cancer cell heterogeneity. The second model assumes that tumors resemble perturbed normal tissues, which are organized in a hierarchical manner, with slowly dividing, self-renewing stem cells that give rise to a highly proliferative cell population. Both models account for the fact that only a subset of cells has a

tumor initiating capacity. The difference lies in the origin of this feature. In the stochastic model every cell within a tumor can potentially acquire this phenotype, so the tumor initiating potential depends on intrinsic or extrinsic factors. In contrast, in the hierarchical model there is only a subset of cells possessing unique biological properties that allow them to initiate tumor growth.

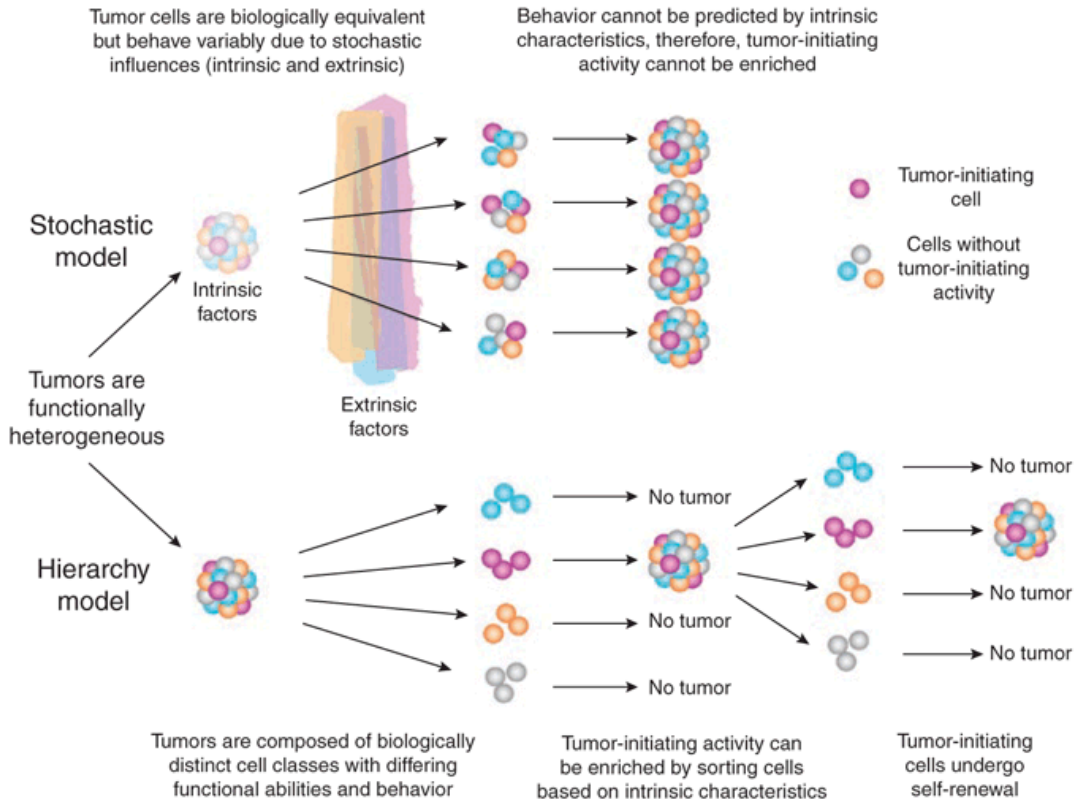

Figure 1. Comparison of hierarchical and stochastic models of cancer [3]

Leukemia was the first cancer type in which the cell heterogeneity was observed [3]. The first proof of hierarchical organization of cancer cells also came from leukemia, were cancer stem cells (CSC) were discovered [4, 5]. More recently CSC were isolated from many solid tumors, including brain, breast and colon cancer [6-9]. Those discoveries support the model of cancer in which slowly proliferating cancer stem cells give rise to bulk tumor cells of high but limited proliferative capacity. In this regard CSC share some features with normal tissue stem cells: through asymmetric cell division they give rise to both stem cells and more differentiated cell and are thereby able to renew the stem cell pool and to produce more proliferative progeny; upon injection into immunocompromised mice CSC initiate tumor formation, in which both CSC and their differentiated progeny are present. The similarity of

CSC to normal stem cells is also reflected in their gene expression profiles [10], which is responsible for frequently observed protein expression similarity between these cell types. For instance, multidrug transporters of the ABC-cassette family can be found both in CSC and normal stem cells, providing protection of stem cells from cytotoxic agents and, in the case of CSC, rendering them resistant to chemotherapy. Convergent expression of stem cell associated proteins by CSC does not necessarily mean that CSC arise from normal stem cells undergoing malignant transformation. It is also possible that they are derived from more committed cells in a process of de-differentiation. Whatever the origin of CSC, it seems likely that their presence in a multitude of cancers is responsible for disease relapse, as they respond poorly to chemo- or radiotherapy. Therefore, for therapeutic purposes it is important to better understand the molecular mechanisms governing CSC.

Expression of various cell surface proteins was used to isolate CSC from solid tumors (Table 1). One of the first markers, shown to discriminate between CSC and differentiated cancer cells was CD44 [11]. In breast cancer its presence combined with absence of CD24 was shown to select for cells able to recapitulate a phenocopy of the original tumor upon xenotransplantation [7]. Cells isolated from primary prostate tumors or metastases that express CD44, but also high levels of integrin $\alpha_2\beta_1$ and CD133, had increased tumorigenic potential *in vitro* [12]. In ovarian cancer CSC have been identified by CD44 and CD117 expression [13].

The panel of CSC markers is growing, but controversies have arisen around the use of some of them. Isolation of CSC based on CD133 expression has yielded contradicting results, as several groups have shown that $CD133^-$ cells can also be tumorigenic [2]. The tumorigenic potential of $CD133^+$ cells could be cancer type specific, but the use of different antibodies for the same marker in CSC isolation protocols can also be the cause of the opposing results. The use of cell surface markers for CSC isolation has also been questioned because their expression is not constant. Thus, the above mentioned CD133 expression can be modulated by hypoxia [14]. Other CSC markers seem to be specific only for certain cancer types, like ABCB5 and ABCG2, used in melanoma CSC isolation, which do not distinguish CSC populations in colon, breast and prostate cancer [2]. Moreover, combinations of different markers and their increasing numbers render it more difficult to find a unified protocol for CSC isolation.

Tumor type	CSC marker	Tumor cells expressing CSC marker (%)	Minimal number of cells expressing CSC markers for tumor formation
Breast	$CD44^+/CD24^{-/low}$	11 - 35	200
Breast	$CD44^+/CD24^-$	ND	2000
Breast	$ALDH1^+$	3 - 10	500
Brain	$CD133^+$ (GBM)	19 - 29	100
	$CD133^+$ (MB)	6 - 21	100
Brain	$CD133^+$	2 - 3	500
Colon	$CD133^+$	1.8 - 25	200
Colon	$CD133^+$	0.7 - 6	3000
Colon	$EpCAM^{hi}/CD44^+$	0.03 - 38	200
Head and neck	$CD44^+$	0.1 - 42	5000
Pancreas	$CD44^+/CD24^+/ESA^+$	0.2 - 0.8	100
Pancreas	$CD133^+$	1 - 3	500
Lung	$CD133^+$	0.32 - 22	10000
Liver	$CD90^+$	0.03 - 6	5000
Melanoma	$ABCB5^+$	1.6 - 20	1000000
Mesenchymal	Side population (Hoechst dye)	0.07 - 10	100

Table 1. Prospective isolation of human CSC from freshly dissociated solid tumors; ALDH – aldehyde dehydrogenase; EpCAM – epithelial cell adhesion molecule; ESA – epithelial specific antigen; GBM – glioblastoma multiforme; MB – medulloblastoma; ND – not determined; modified from [15]

Another way for CSC isolation is the dye exclusion assay. This assay is based on the expression of ABC transporters on putative CSC. Upon staining with Hoechst 33342 the ABC transporters pump the dye out of the cell, creating Hoechst negative side populations (SP) containing CSC. SP based isolation of CSC has been used in glioblastoma, melanoma, in breast and lung cancers [16]. However, contradicting results came from subsequent studies on thyroid, adrenocortical and glioma CSC, showing that non-SP cells can generate SP cells and that they are equally proliferative and tumorigenic [17-19]. Furthermore, SP size has been shown to depend on density of cell culture and Hoechst concentration [2] and the mutagenic and carcinogenic potential of the dye renders it less reliable for CSC isolation.

The debate over the use of different methods for CSC isolation remains open. However, increasing numbers of stem cell markers allow studying the best possible combinations specific for CSC from different cancer types. Yet, the most reliable markers would be the cell surface proteins specifically expressed by CSC and at the same time playing a vital role in CSC biology. Thus, it is crucial to decipher the functional relevance of those proteins in CSC. Further characterization of the molecular pathways governed by the stem cell markers is also necessary for developing CSC-targeted therapy.

This thesis is composed of two CSC-related projects. The first aims at identifying new biological features of the CSC marker CD44 and was described in the article “Transportin regulates nuclear import of CD44” published on October 1st 2010 in the Journal of Biological

Chemistry. The second project investigates the role of the oncofetal protein Imp2 in glioblastoma cancer stem cells, resulting in a manuscript entitled “Oxidative phosphorylation regulated by Imp2 is crucial for glioblastoma cancer stem cells”.

PART 1: Nuclear translocation of CD44

Introduction

Before CD44 had been associated with cancer stem cells, it had been extensively studied in various cellular contexts. First, it was demonstrated to be cell surface extracellular matrix receptor [20]. Its expression has been observed in most normal tissues [21], yet higher levels of CD44 and its splicing variants correlate with cancer progression and metastasis [22]. Association of CD44 with metastasis and the cancer stem cell phenotype has renewed interest in its molecular functions.

The CD44 protein is encoded by a gene that comprises 20 exons [23]. The most abundant form of CD44 is derived from a transcript containing exons 1-5, 16-18 and 20. This standard form of CD44 (CD44s) is translated into a 341aminoacid (aa) molecule that can be divided into three domains: a N-terminal extracellular domain (248aa), a transmembrane domain (23aa) and a C-treminal cytoplasmic domain (70aa). Due to cell context dependent N- and O-glycosylation of its extracellular domain the molecular size of CD44s can vary. Taking into account all the possible splicing variants and glycosylation combinations over 800 isoforms of CD44 could be generated, yet not all variants are expressed [22].

The principal function of CD44 is binding to hyaluronic acid (HA), an important component of the extracellular matrix (ECM) [20]. Binding of HA is crucial for CD44 mediated motility and can be modulated by intracellular signaling as well as CD44 ectodomain cleavage [24]. In addition to HA binding CD44 can activate integrins, modulating cellular adhesion [23]. Another function of CD44 is assembling MMP7 and MMP9 with their substrates on cell surface. Only when bound by CD44, can MMP9 activate TGF-β, which triggers neovascularization [25]. Similarly, binding of MMP7 to CD44 allows it to cleave heparin-binding epidermal growth factor, which also upon interaction with CD44 activates pro-survival signaling [26].Those interactions can be further enhanced by CD44-ERBB4 complexing [26]. It is the ectodomain of CD44 that mediates these interactions. However, the intracellular part of the HA receptor is also biologically active. Via interaction with ezrin, radixin and moesin (ERM) proteins and Merlin, CD44 is linked to actin cytoskeleton, influencing local cytoskeletal reorganization, as well as CD44-mediated Ras signaling [23, 27]. ERM proteins also mediate CD44 control over the Hippo pathway linked to stress induced apoptosis [28]. Moreover, the intra-membrane cleavage of CD44 can release the intracellular domain, which is translocated to the nucleus and activates gene transcription [29]. The broad spectrum of CD44 protein interactions makes it an important player in various

cellular processes. Those distinct functions are orchestrated by different isoforms of CD44, generated by mRNA splicing and glycosylation. Since so many isoforms of CD44 can be present in different cell types, it is possible that there are still many functions of this protein to be uncovered.

Intracellular signaling mediated by CD44 has primarily mitogenic and anti-apoptotic effects. Yet, the main biological process in which CD44 is involved is adhesion. By binding to extracellular matrix components and mediating interactions with integrins and ERM proteins, CD44 controls cytoskeleton remodeling, influencing cell shape and motility. Thus, it is crucial for events such as wound healing, lymphocyte homing, but also normal embryonic development and invasion of cancer cells [23]. Overexpression of CD44 can be highly advantageous for cancer cells, as it allows them to migrate, increases their proliferation by Ras signaling and inhibits apoptosis by interacting with and activating receptor tyrosine kinases.

High expression of CD44 has been used to isolate CSC from hematopoietic and solid malignancies, including breast, prostate and colon cancer [11]. The frequency of CD44 expression in CSC from different tumors reflects its functional importance in those cells. Leukemia stem cells secrete HA, that stimulates their homing to the endosteal niche where normal hematopoietic stem cells also reside [30]. Expression of CD44 on both cell types is crucial for their homing [31], but also for CXCL12-dependent transendothelial migration, that facilitates engraftment in the niche [30]. Cancer stem cell niches in solid tumors are not yet well studied. Nevertheless, it is possible that the adhesive function of CD44 enables the interplay between solid tumor stem cells and their microenvironment. However, in breast cancer the HA-CD44 interaction seems to regulate epithelial-to-mesenchymal transition (EMT), rather than interaction with the CSC niche [11]. There have also been reports of CD44 and its variants governing expression of genes associated with stemness, including NANOG and MDR1 (also important for multidrug resistance of CSC)[32] and CD44 being a target of the stem cell signaling pathway Wnt [33]. Therefore, despite the fact that CSC can be isolated from different tumor types with the same marker, the functions that this molecule plays might still remain cell-specific.

At least part of the signal transduction governed by CD44 upon ligand binding is conducted through receptor internalization. A fraction of internalized receptor undergoes proteolytic cleavage, which generates the intracellular domain (ICD) (Fig.2) [24, 34]. The ICD is then translocated to the nucleus where it participates in regulation of gene transcription

[29]. However, in our laboratory an observation was made, that also a full-length CD44 protein could be found in the nucleus.

The aim of this project was to validate the nuclear localization of full-length CD44, to study the mechanism of its translocation and to find its putative function.

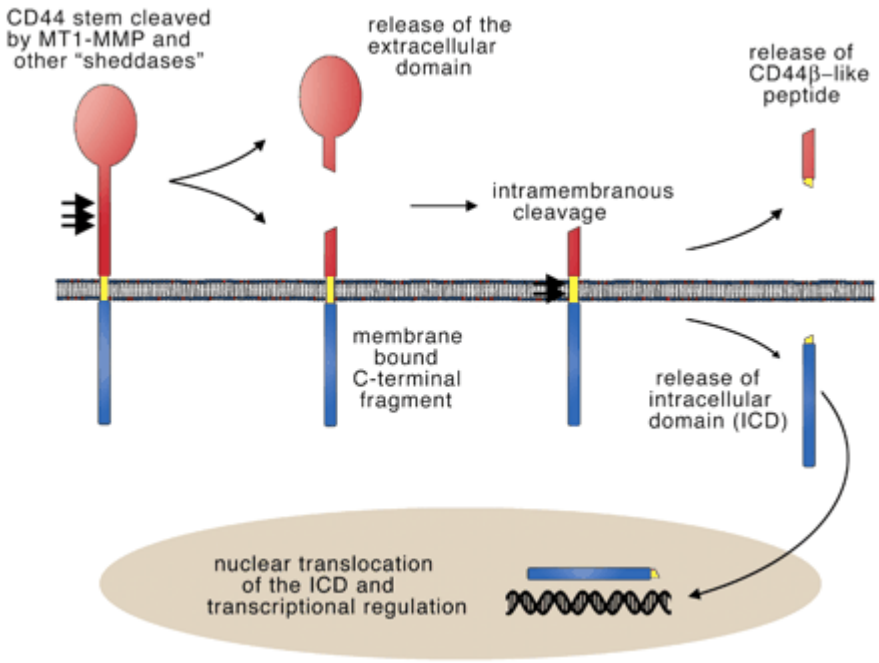

Figure 2. CD44 sequential cleavage [24]

Results summary

Using an antibody that recognizes the extracellular domain of CD44 an immunofluorescent staining was performed on several cell lines. Clear nuclear staining was observed in all tested cell lines, regardless of the tumor type or tumorigenicity. Since the antibody used in this assay does not discriminate between cleaved and full-length form of CD44, immmunoprecipitation of CD44 was performed, using the nuclear fraction of human osteosarcoma cells MNNG/HOS, that endogenously express large amounts of the standard form of CD44. This experiment confirmed the presence of full-length CD44 in the nucleus.

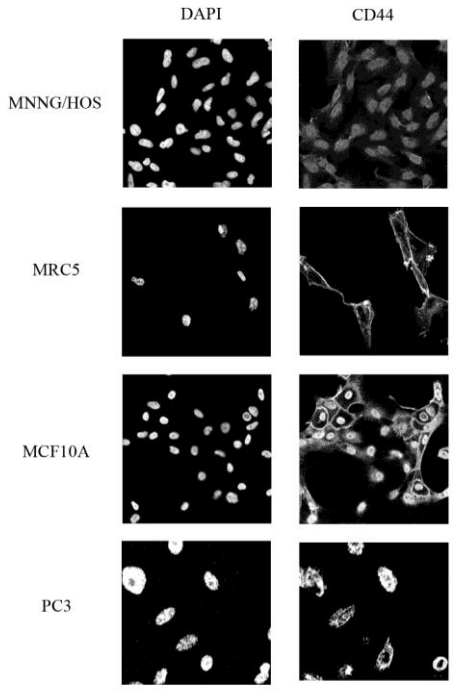

Figure 3. *Nuclear localization of CD44;* immunofluorescence staining of CD44 in the indicated cell types; nuclei stained with DAPI;

To determine whether nuclear localization is a result of HA receptor internalization from the cellular membrane or if *de novo* synthesized CD44 is translocated directly from the cytoplasm, CD44 immunoprecipitation from nuclear extracts was preceded by cell surface biotinylation. Detection using streptavidin revealed that the precipitated CD44 band was also highly biotinylated, confirming membrane origin of nuclear-localized receptor. This result was later confirmed by endocytic pathway inhibition using nocodazole, that resulted in a decrease in nuclear staining of the HA receptor. Moreover, overexpression of a mutant CD44 that lacks signal peptide, necessary for its membrane localization, showed lower level of nuclear localization of the protein, underlining the importance of membrane localization for nuclear translocation.

In search for potential protein partners of CD44 which could provide insight into the mechanism of its nuclear translocation and its intracellular signaling, a pull-down assay was performed. In this assay a large scale immunoprecipitation of CD44 from the cytoplasmic fraction was followed by mass-spectrometry analysis. As a result, several proteins of the karyopherin family were identified. The interactions between CD44, importin β, transportin1 and exportin Crm1 were validated by Western blotting.

Functional validation of the observed interactions was assessed in nuclear import assays. Permeabilized, cytosol depleted cells were incubated with cytosolic fractions devoid

of import factor or containing an import inhibitor and the influence of those conditions on nuclear CD44 localization was measured (Fig. 4A). Importin β depletion from cytosolic extracts used in the assay did not influence CD44 localization. However, addition of transportin1 inhibitor, peptide M9M [35], significantly reduced CD44 amount in the nuclei. These results suggested that CD44 is imported to the nucleus by transportin1. To investigate whether export of the HA receptor is mediated by exportin Crm1, an inhibitor, leptomycin B, was added to the cells in culture and CD44 localization was monitored over time (Fig. 4B). After 4h of treatment an accumulation of nuclear CD44 was observed, implicating exportin Crm1 in its trafficking.

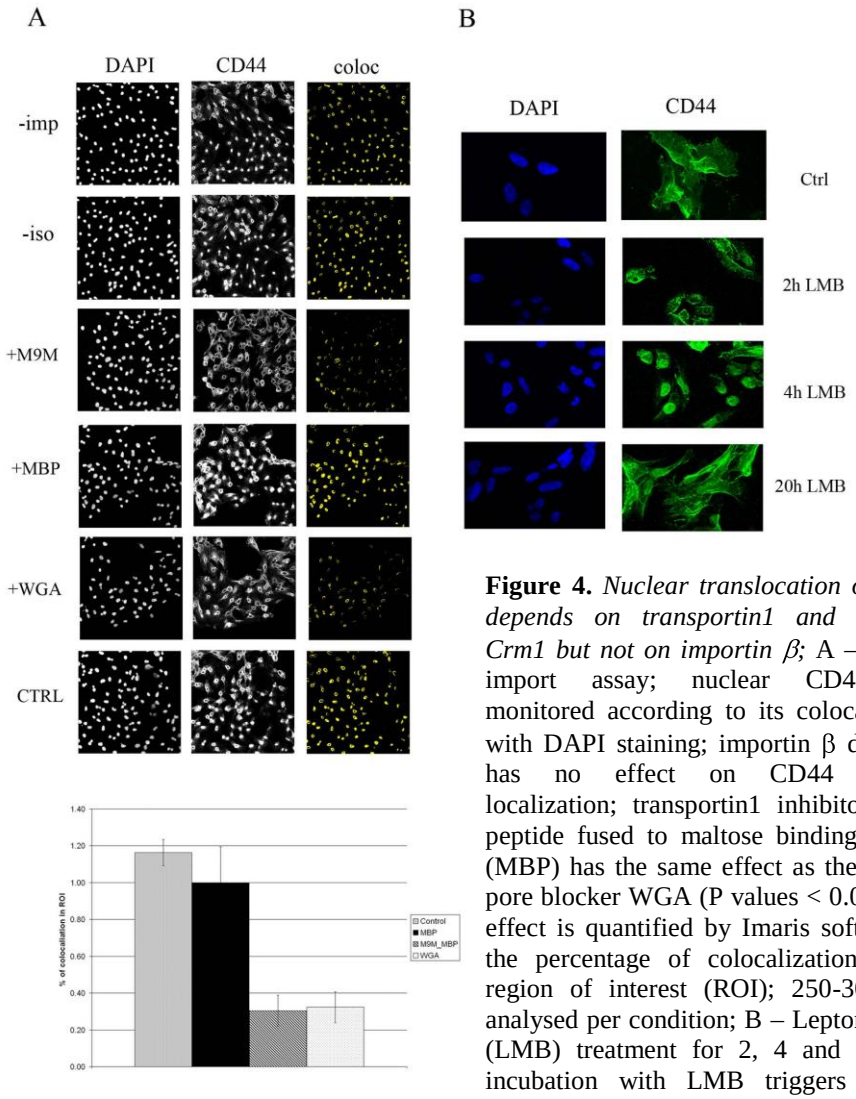

Figure 4. *Nuclear translocation of CD44 depends on transportin1 and exportin Crm1 but not on importin β;* A – nuclear import assay; nuclear CD44 was monitored according to its colocalization with DAPI staining; importin β depletion has no effect on CD44 nuclear localization; transportin1 inhibitor M9M peptide fused to maltose binding protein (MBP) has the same effect as the nulcear pore blocker WGA (P values < 0.005); the effect is quantified by Imaris software as the percentage of colocalization in the region of interest (ROI); 250-300 cells analysed per condition; B – Leptomycin B (LMB) treatment for 2, 4 and 20h; 4h incubation with LMB triggers nuclear accumulation of CD44.

Further characterization of nuclear translocation of CD44 required determination of its nuclear localization signal (NLS). Since both the full-length CD44 and its ICD can be translocated to the nucleus, the potential nuclear localization signal should be present in the

cytoplasmic domain of the protein. Therefore, three mutants were constructed, each lacking a different portion of this domain. One of the mutants, t-20, was lacking the first 20aa of the cytoplasmic domain, which shared high similarity with the predicted NLS recognized by transportin1 [36]. Both the t-20 and a mutant with the deletion of the whole cytoplasmic domain had an impaired nuclear localization. Interestingly, the t-20 mutant CD44 was still able to bind transportin1, as revealed by immunoprecipitation.

The next issue was the function that full-length CD44 could play in the nucleus. Knock-down of CD44 in an osteosarcoma cell line resulted in decrease of *de novo* RNA polymerization, measured by incorporation of bromouridine (BrU) (Fig. 5 A-C). The same result was observed in fibroblasts isolated from CD44 knock-out mice (Fig. 5D).

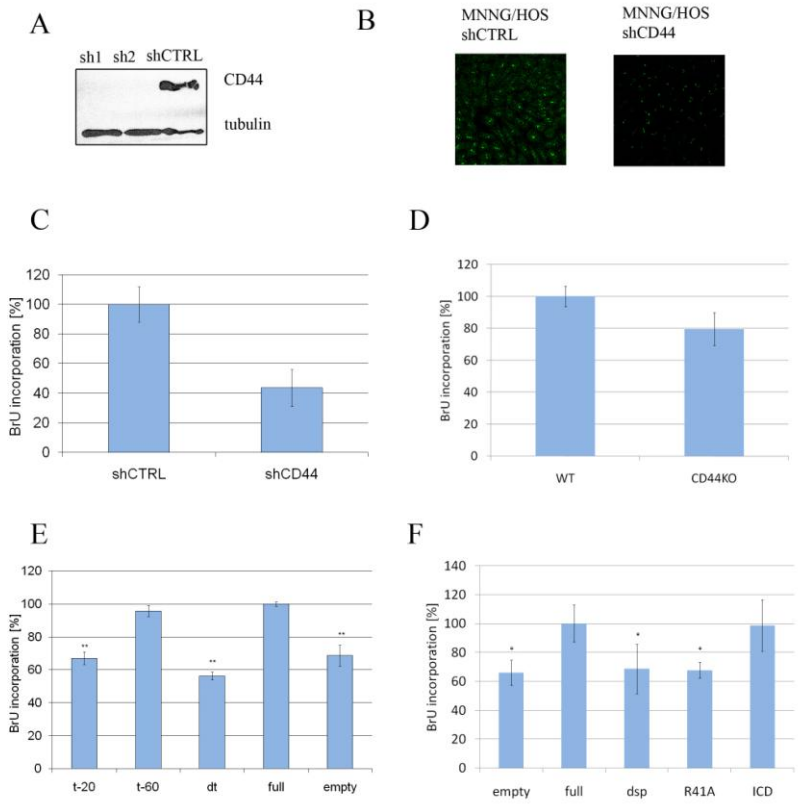

Figure 5. *Nuclear CD44 enhances RNA synthesis;* A – shRNA downregulation of CD44 expression; Immunofluorescence – B – and a colorimetric assay - C – show weaker BrU incorporation in cells depleted of CD44 compared to control cells (mean of three experiments, P value *<0.05); D – A similar effect is observed in colorimetric assays with CD44-/- mouse fibroblasts compared to the wild-type cells (mean of three experiments, P value <0.05); E - MC CD44t-20 mutant incorporates less BrU that the wild type and the CD44t-60 mutant as assessed by the colorimetric assay (mean of three experiments, t-test comparison of mutants to WT - P values *<0.05; ANOVA P value is 0.005593); F – The role of extracellular domain in BrU incorporation; representative graph of the colorimetric assay; lack of the signal peptide (dsp) or R41A hyaluronian- binding site mutation decreases BrU incorporation (representative experiment, t-test comparison of mutants to WT - P values * <0.05; ANOVA P value is 0.025);

What is more, the expression of the mutants that did not localize to the nuclei also decreased BrU incorporation levels (Fig. 5E-F). The control over RNA polymerization could be dependent not only on nuclear localization of CD44, but also on HA binding. This notion is

supported by the fact that cells expressing a mutant unable to bind HA also had lower levels of BrU incorporation, despite the proper nuclear localization of this mutant (Fig. 5F).

The main findings of this work were:

- Full-length CD44 can be found in the nucleus
- Full-length CD44 is translocated from the membrane via endocytic pathway, imported to the nucleus by transportin1 and exported by exportin Crm1
- Identification of nuclear localization signal bound by transportin1
- Full-length CD44 in the nucleus enhances overall RNA synthesis

Discussion and perspectives

Previously, it has been described that CD44 upon ligand binding undergoes sequential trimming by several proteases [34]. The ectodomain cleavage releases soluble CD44, which is associated with the metastatic phenotype [34]. Subsequent intramembrane cleavage of CD44 produces the ICD, which is translocated to the nucleus where it activates gene transcription. This shedding of CD44 is crucial for efficient turnover of the protein and for cell migration into the extracellular matrix. However, the present work demonstrates that also full-length CD44 can be found in the nucleus and that it is important for the RNA polymerization. The remaining question is whether the ICD and full-length proteins have redundant functions. Generation of ICD can be stimulated by TPA treatment (12-O-tetradecanoylphorbol 13-acetate) [37], but in the cells used in this work CD44 cleavage was not induced. Therefore, it is plausible that in some cells, where generation of ICD is not active, translocation of full-length CD44 may be preferable.

The present work focuses on the mechanism by which CD44 is translocated to the nucleus. It describes proteins responsible for nuclear trafficking of CD44. Interestingly, the mutant of CD44 that lacks the first 20aa of the cytoplasmic tail cannot be imported to the nucleus although it still binds to transportin1. This issue can be explained by the properties of transportin1. Within the NLS of its cargo, transportin1 recognizes two sites, A – a high affinity binding site at the C-terminal part of the NLS and B – at the N-terminus of the NLS, a site responsible for conformational changes in transportin1 and dissociation of the cargo in the nucleus (Fig. 6) [38]. Site A corresponds to residues DRKPS, which were not deleted in the t-20 mutant. Therefore, the results obtained with this mutant show that site A of the NLS is

sufficient for CD44-transportin1 interaction, but the nuclear translocation cannot occur without the CD44 fragment containing the B site.

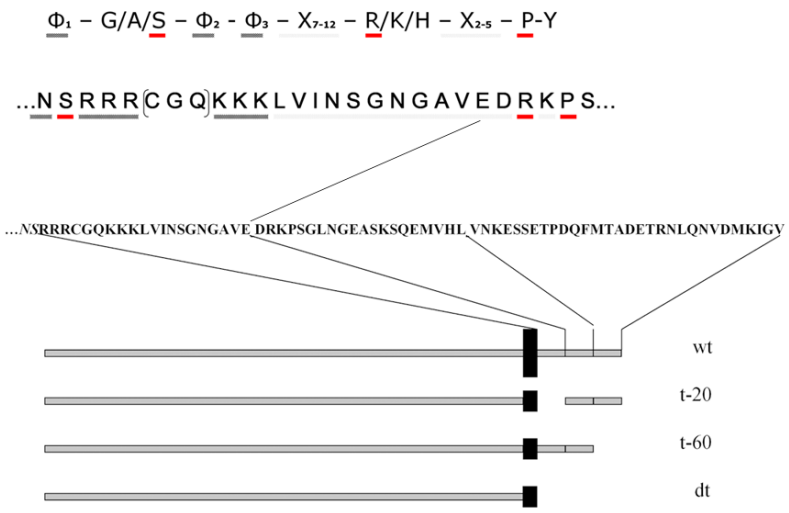

Figure 6. *CD44 contains a transportin1-specific nuclear localization sequence (NLS);* predicted sequence of transportin1 recognized NLS (upper line) corresponds to sequences present in the cytoplasmic domain of CD44; lower panel – the major portion of predicted NLS is deleted in CD44t-20 mutant (middle line); the DRKPS fragment corresponds to site A recognized by transportin1; the NSRRR(CGQ)KKK fragment corresponds to transportin1 binding site B;

It has been previously shown that ICD of CD44 activates gene transcription. Thus, the nuclear translocation of the full-length protein could have a similar function. Indeed, measuring BrU incorporation into nascent RNA showed its dependence on nuclear localization of HA receptor. Interestingly, a mutation in HA binding site disables this function. Hyaluronan has been previously found in the nucleus [39], thus it is plausible that nuclear delivery of the CD44-HA complex is important for RNA synthesis. The direct interaction of CD44 with RNA polymerase was excluded in co-immunoprecipitation attempts, yet an indirect mechanism is possible. The analysis of protein interactors of nuclear CD44, based on pull-down from the nuclear fraction and mass-spectrometry, revealed several potential candidate proteins that could mediate this function, including Arp2/3 and SWI/SNF. Arp2/3 is an actin-binding protein, involved in actin filament polymerization and cytoskeleton remodeling [40]. However, this protein has also been found in the nucleus where it regulates RNA polymerase II-dependent transcription [41]. Both Arp2/3 and CD44 can be linked to actin filaments, therefore it would be of interest to know whether the observed effect of CD44

on RNA synthesis could also depend on nuclear actin and its interactors. Nuclear SWI/SNF complex controls transcription by chromatin remodeling [42]. Interestingly, it has been shown that BRG-1 subunit of this complex regulates CD44 expression [43]. Therefore, it could be that CD44 creates a feedback loop, controlling its own expression via the SWI/SNF complex. Further characterization of the interactions between CD44 and nuclear proteins involved in RNA synthesis could reveal new mechanisms and potential new functions of the HA receptor. It would be also of interest to investigate whether there are any specific transcripts that are increasingly synthesized in the presence of nuclear CD44.

Another point not discussed in this study is the significance of nuclear CD44 in cancer. Although the nuclear localization seemed not to be cell type restricted and did not correlate with the metastatic potential of tested cancer cell lines, it might be that nuclear CD44 has different targets in different cancer cells. Since its expression is often associated with malignant phenotype and cancer stem cells, the nuclear function of full-length CD44 associated with RNA synthesis may affect pathways important for tumorigenesis.

Original article

PART 2: Imp2 in glioblastoma stem cells

Introduction

One of the first discoveries of CSC in solid tumors was the isolation of CD133 expressing cells from the glial brain tumor, glioblastoma multiforme (GBM) [6]. It has been shown that upon xenotransplantation only the CD133+ subpopulation, comprising 19-22% of tumor cells, was able to recapitulate the parental tumor, containing both CD133+ and CD133- cells. This discovery initiated a wide search for CSC in solid malignancies, with CD133 as CSC marker. Several other cell surface proteins have also been shown to enrich CSC populations in GBM, including SSEA1[44] and CD44 [45].To avoid the bias from heterogeneous protein expression, GBM CSC can also be isolated based on their similarities to normal neural progenitor cells. Both the CSC and neural stem cells (NSC) under specific culture conditions form neurospheres *in vitro*. Studies of GBM CSC are therefore a valid source of methods used in the CSC field, as CD133 and neurosphere formation are widely used in CSC research.

Glioma is the most common primary brain tumor, diagnosed in 5 per 100000 persons each year [46]. Glial tumors can be divided into histological subtypes including astrocytoma, oligodendroglioma and mixed oligoastrocytoma. This division is based on histological similarities between tumor cells and normal glial cells (astrocytes and oligodendrocytes) [46]. Gliomas comprise a spectrum of low to high grade malignancies, where low-grade tumors often progress to a higher grade [46]. The most malignant type of glioma is glioblastoma multiforme (GBM), accounting for over 51% of all gliomas diagnosed in adults [47]. GBM is associated with extremely poor prognosis with median survival of 9-14 months, despite the aggressive therapy including surgery, chemotherapy and radiation.

At the histopathological level GBM can be described as a tumor of poorly differentiated neoplastic astrocytes, with cellular and nuclear atypia and characteristic pseudopallisading necrosis [46]. Yet, within a given tumor major heterogeneity is often observed, particularly regarding expression patterns of transcriptional regulators, tumor-suppressor proteins and kinase mutations [48]. Different entities of a tumor correspond to a divergent clonal expansion of tumorigenic cells. These observations raised the question of the cell of origin of GBM. Initially, it was thought that GBM originates from astrocytes. However, the first step of transformation requires cells to proliferate whereas in adult brain glial cells do not divide, unless a reactive proliferation is required [48]. Since there is no link between

events such as head trauma that could stimulate reactive proliferation of glial cells and the incidence of glioma development, the astrocytic origin of GBM is unlikely. Further research focused on identification of normal brain stem cells have led to isolation of neuroectodermal stem cells in the subventricular zone band in the human brain, multipotent cells that displayed astrocytic characteristics [49]. It is therefore more likely that those proliferative, migratory and undifferentiated cells can undergo transformation and give rise to malignant glioma [50]. Glial progenitor cells have been shown to be more permissive to oncogenic transformation than more mature astrocytic cells and upon expression of Ras and Akt oncogenes they gave rise to GBM-resembling tumors in mouse brain [51]. Moreover, neural progenitor cells express the CSC marker CD133, supporting the stem/progenitor cell origin of GBM [52].

Cancer stem cells, the dormant driving force of a tumor, resemble stem cells of a developing tissue, often re-expressing proteins restricted to embryonic tissues that are absent in mature cells. One of the oncofetal proteins that is important for normal brain development, highly expressed by several malignancies, but present only at low level in a few adult tissues is insulin-like growth factor 2 mRNA binding protein (Imp2, IGF2BP2) that belongs to Imp/VICKZ protein family [53]. Studies on chicken and Xenopus paralogues of Imp2 have shown their implication in mRNA localization, translation and stability [54]. Human Imp1 and Imp3 have been associated with poor outcome in various malignancies, including pancreatic adenocarcinoma, prostate carcinoma, thyroid carcinoma, breast cancer, colon carcinoma, melanoma and ovarian cancer [55]. However, no underlying molecular mechanism has been found. Recently several studies provided new insight into Imp2 biology, showing its implication in type 2 diabetes [54], smooth muscle cell adhesion and motility [56] and overexpression in different cancer types [55].

Taking into account the expression patterns of Imp2 – its importance for normal brain development [57], silencing in adult brain and re-expression in malignancies has made it an interesting target for investigation. Therefore, we sought to determine Imp2 expression and functional relevance in GBM CSC.

During this investigation new observations concerning CSC metabolism were noted. Since cancer is a disease of abnormal proliferation, cancer cells have high energy demands to support their growth and survival. The primary way of energy production in any cell is to metabolize glucose to carbon dioxide via generation of pyruvate in glycolysis and its oxidation in mitochondrial tricarboxylic acid cycle (TCA)[58].

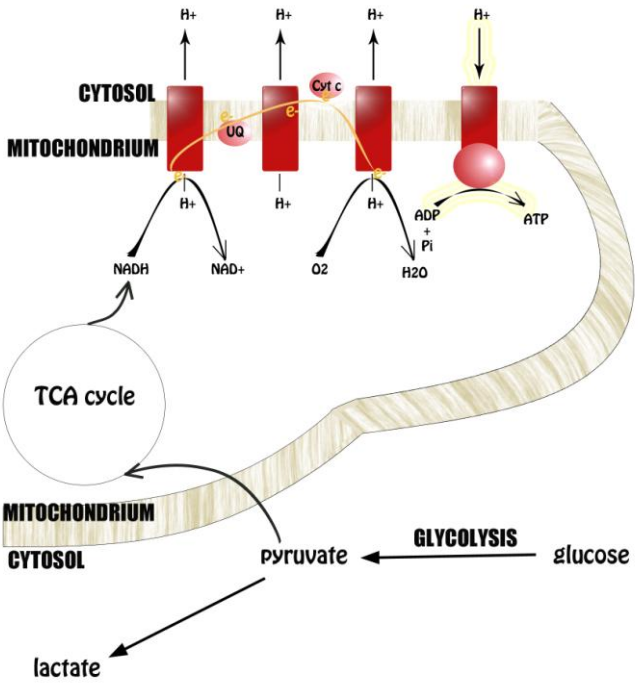

Figure 7. Glucose metabolism fuels ATP production; Pyruvate, produced during glycolysis can be transported to the mitochondria, where it fuels TCA cycle and NADH production; NADH oxidation is an electron source for the oxidative phosphorylation chain; the electron transport forces the extrusion of protons from the mitochondria, creating a transmembrane potential; this potential energy, the proton motive force, is then used for the ATP synthesis;

The by-product of TCA, NADH is used as electron donor for the oxidative phosphorylation chain, where electrons are transferred via respiratory chain complex proteins I-IV to oxygen, proton gradient across the mitochondrial membrane is established and used to fuel ATP synthesis (Fig. 7). This chain of events allows for production of 36 moles of ATP per mole of glucose. However, this efficient synthesis of ATP requires constant glucose and oxygen supply. Since in a growing tumor increasing distance from the vascular capillaries can lead to local hypoxia and decrease in glucose availability, cancer cells have developed another strategy to support their rapid proliferation. In the process of anaerobic glycolysis, independent of oxygen supply, glucose is metabolized to pyruvate, which instead of being directed to the TCA cycle, is used for lactate production (Fig. 7). Although it seems wasteful, as most of the lactate is excreted from the cell, a by-product of this reaction is NADPH required for macromolecule synthesis. Therefore, although anaerobic glycolysis yields only 2-4 moles of ATP per mole of glucose, it generates building material for macromolecules required for cellular proliferation. This process is also faster, enhancing the rapid growth of a tumor. Yet, it is not clear if all tumor cells switch to anaerobic glycolysis and, what is more

interesting, if cancer stem cells are also metabolically different from the bulk tumor counterparts.

Results summary

In order to determine the expression of Imp2 in glioblastoma an immunohistochemical staining of normal brain, low grade gliomas and 50 cases of GBM were compared (Fig. 8A). Imp2 is absent in normal brain and in low grade gliomas, but 75% GBM cases revealed moderate to high levels of Imp2 staining. The result was confirmed by bioinformatic analysis of Sun database [59], showing a correlation between glioma grade and Imp2 expression (Fig. 8B). The expression of Imp2 was increased in GBM CSC, as shown by real-time Q-PCR in CD133+ cells compared to CD133- counterparts and by immunofluorescence in neurospheres compared to adherent, differentiated GBM cells.

To establish the importance of Imp2 expression in GBM CSC a shRNA was designed and delivered to the GBM primary cultured cells grown as neurospheres. Effective silencing of Imp2 has decreased GBM CSC sphere formation capacity and tumorigenesis (Fig. 8 C-D).

Next, Imp2 immunoprecipitation was performed, to pull down Imp2-bound mRNA species and Imp-2 interacting proteins, that are present in ribonucleoprotein particles. Again, primary cultures of GBM CSC were used for the experiment. Microarray analysis of the transcripts, as well as mass-spectrometry of Imp2 interactors revealed that there is an overrepresentation of mitochondria related molecules. In the transcript analysis a significant proportion of mRNAs that are associated with mitochondrial functions were found. Protein interactor analysis revealed that Imp2 binds several subunits of respiratory complex I, all involved in early steps of complex I assembly.

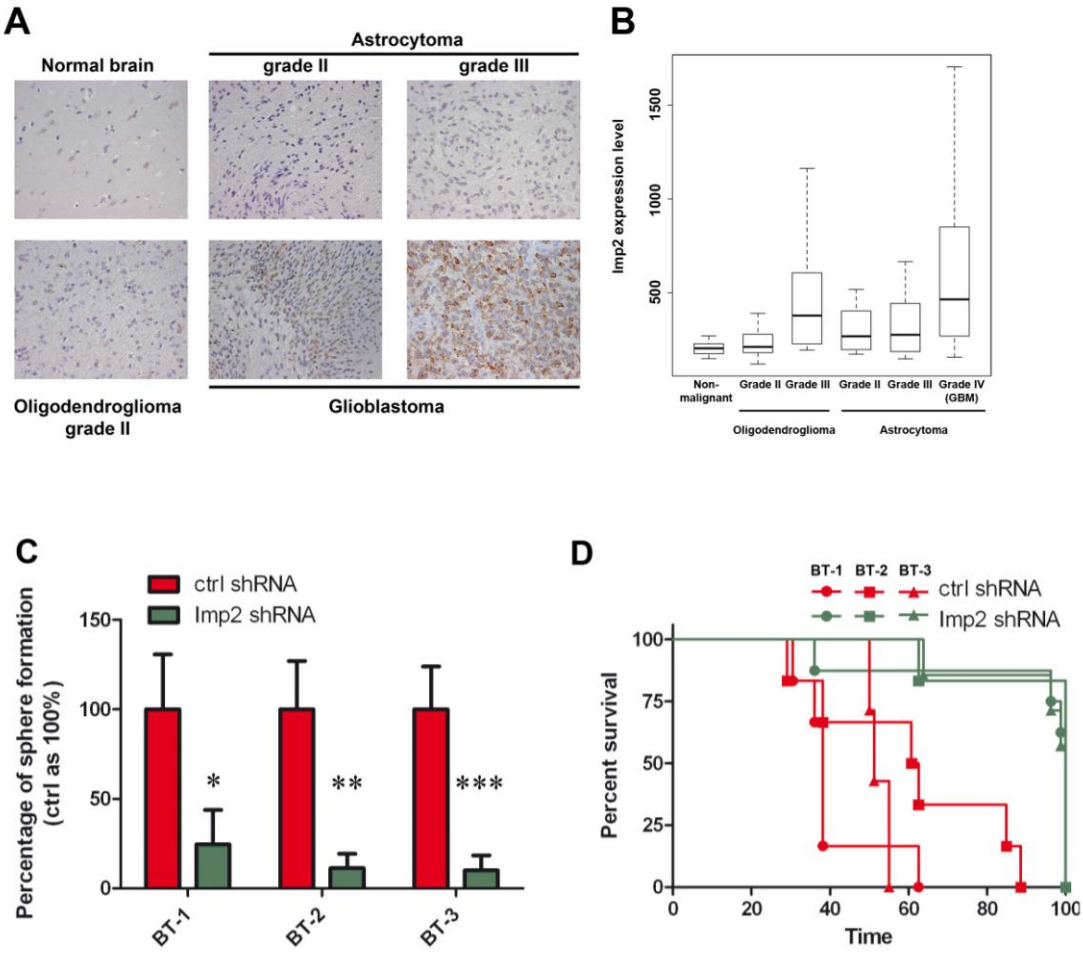

Figure 8. Imp2 expression in GBM and its implication in GBM CSC self-renewal and tumorigenicity; A - immunohistochemical staining of paraffin sections shows lack of Imp2 expression in normal brain and low grade gliomas and a spectrum of positive staining in GBM ; B — Imp2 expression across gliomas of different grade in an independent data set (Sun et al) ; t-test P values : GBM vs normal: p=9.678e-11; GBM vs grade II/III oligodendroglioma: p =0.006351; GBM vs grade II/III astrocytoma: p =4.310e-05; C - Stable Imp2 shRNA expression impairs sphere formation in three batches of GBM CSC (BT-1, BT-2 and BT-3; * - P value 0.0227, ** - P value 0.0015, ***- P value 0.0008, unpaired two-tailed t-test); error bars represent standard deviations; D – Imp2 shRNA expression diminishes GBM CSC tumor forming capacity; the experiment was repeated in three batches of cells (circles, squares and triangles); 6 animals were used per condition; since tumor formation by different BTs varied over time, a timescale of the experiment is presented (with the final time point as 100); the differences between Imp2 and ctrl shRNA expressing cells for each cell batch are significant (Log-rank (Mantel-Cox) test P value for BT-1 is 0.0088, BT-2 is 0.0036, BT-3 is 0.0003);

The interactions of Imp2 with transcripts and proteins involved in oxidative phosphorylation chain pointed to its influence on the mitochondrial activity of GBM CSC. Knock-down of Imp2 impaired mitochondrial activity of those cells (Fig. 9), had an important effect on oxygen consumption and enzymatic activity of respiratory complex I.

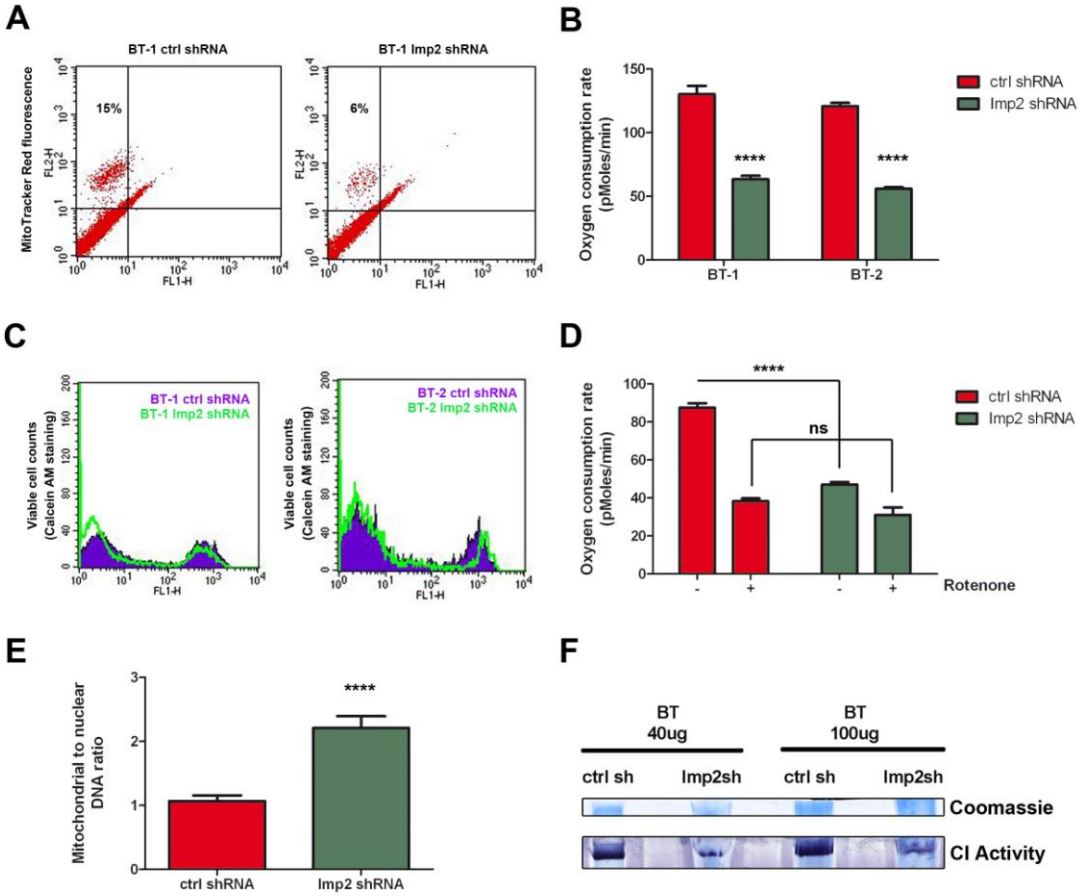

Figure 9. *Imp2 depletion affects oxidative respiration in GBM CSC*; A – MitoTracker Red staining of active mitochondria decreases in cells depleted of Imp2; representative graphs of 3 experiments with different cell batches are shown; B – diminished oxygen consumption rate (OCR) is caused by Imp2 shRNA expression in two cell batches (BT-1 and BT-2); **** - P value < 0.0001 (paired two-tailed t-test); error bars represent standard deviation; C - Calcein AM staining was performed immediately after OCR measurement to ensure equal seeding of viable cells for the oxygen consumption measurement; D – 1μM rotenone injection decreases OCR of ctrl cells to a level comparable to that measured in Imp2 depleted cells; **** - P value < 0.0001, ns – not significant (two-way ANOVA with Bonferroni's multiple comparison test); error bars represent standard deviation; E - cells depleted of Imp2 accumulate mitochondria; Q-PCR comparison of mitochondrial (16S) to nuclear (18S) DNA content; bars represent mean of two independent experiments on GBM CSC; error bars represent standard deviation; F – respiratory complex I activity is lowered by Imp2 knock-down, as shown by Blue Native PAGE and in-gel activity assay; 40μg or 100μg of the mitochondrial extracts were loaded on the gel;

Gliomas were thought to depend mainly on anaerobic glycolysis as an energy producing pathway [60]. Yet, inhibition of oxidative phosphorylation (OxPhos) had a sever effect on GBM CSC sphere morphology and clonogenic capacity, that resembled the phenotype of Imp2 knock-down cells (Fig. 10). Interestingly, inhibition of anaerobic glycolysis was not affecting the sphere formation.

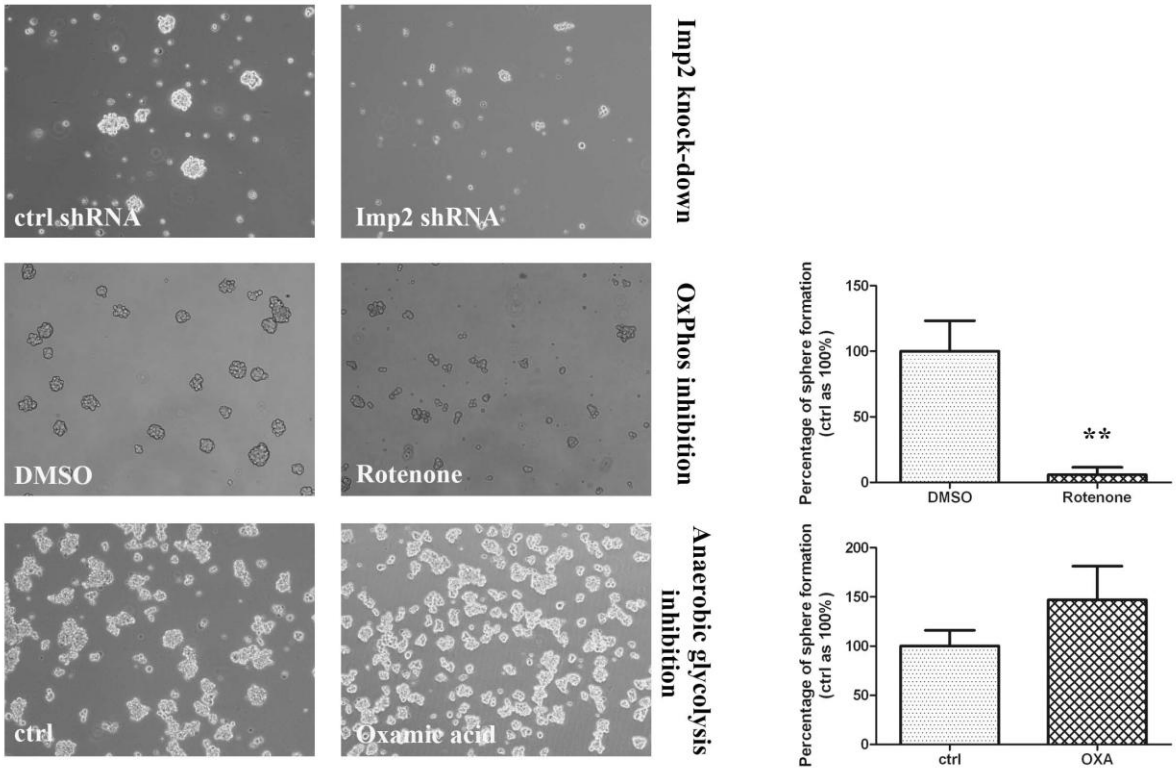

Figure 10. *Inhibition of oxidative phosphorylation impairs clonogenicity and survival of GBM CSC*; silencing of Imp2 affects GBM CSC sphere morphology in the same way as inhibition of oxidative phosphorylation with 1μM rotenone treatment (left panel); the clonogenic potential is diminished by Imp2 shRNA expression (Fig. 8) and by rotenone treatment (upper right panel; ** - P value 0.0024, unpaired two-tailed t-test); anaerobic glycolysis inhibition by 25mM oxamic acid does not significantly affect the clonogenic potential of GBM CSC; representative results for one out of three cell batches are shown; error bars represent the standard deviation;

The main findings of this work were:

- Imp2 expression is restricted to GBM and is high in GBM CSC
- Imp2 knock-down impairs GBM CSC self-renewal and tumorigenic capacity
- Imp2 regulates OxPhos in GBM CSC
- GBM CSC depend on OxPhos, whereas more differentiated cells depend on glycolysis

Discussion and perspectives

Cancer cells develop an array of changes in their genetic, metabolic and histological properties, all of which are connected with increased cellular proliferation. It has been postulated that rapidly dividing cancer cells fulfill their enhanced energetic requirements by glycolysis. Even in the presence of oxygen, cancer cells use glucose to produce only small amounts of ATP, but high levels of lactate and biosynthetic intermediates used to increase the biomass of a tumor. These events, known as the Warburg effect, are often accompanied by mitochondrial gene mutations, which impair mitochondrial respiration. However, an increasing number of studies reveal that oxidative phosphorylation is functional in many tumor types [60, 61]. This preference for OxPhos might be related to decreasing availability of glucose in a growing tumor and an increase of glutamine degradation, a way to fuel OxPhos. The results presented in this work also suggest another explanation for the OxPhos phenotype of some tumors. Since GBM cancer stem cells are highly dependent on OxPhos, it is plausible that overall oxidative potential of a tumor is maintained by high proportion of cancer stem cells and their progeny that still shares the metabolic properties.

Non-transformed cells use OxPhos as the main energy supplying pathway, since it produces more ATP per mole of glucose, the oxygen and nutrient supply is constant. There are not many data about the bioenergetics of normal stem cells. However, there have been reports connecting metabolism and cell differentiation. Higher mitochondrial respiration has been shown to correlate with expression of the neural stem cell marker nestin in cultured neurospheres, suggesting that OxPhos is a hallmark of stem cells [62]. The importance of OxPhos in stem cells has also been confirmed by the observation of higher oxygen consumption rates in embryonic stem cells at early compared to late passages [63]. What is more, active mitochondrial metabolism was shown to discriminate mouse embryonic stem cell potential for teratoma formation [64]. OxPhos activity is also required for transformation of mesenchymal stem cells [65]. These data, together with observation gathered in this work, suggest that mitochondrial respiration can be another common feature shared by normal stem cells and cancer stem cells. The link between OxPhos and transformation of stem cells could also support the hypothesis that CSC are derived from normal stem cells.

Active mitochondrial respiration requires efficient oxygen supply. The Warburg hypothesis suggests that cancer cells use anaerobic glycolysis, independent of oxygen availability. Yet, the results of this work imply that OxPhos is crucial for CSC survival, suggesting that they must also require oxygen. It has been shown by several groups that brain

CSC reside in close proximity to the blood vessels, in a perivascular niche [66-68]. It was also reported that GBM CSC can differentiate to endothelial cells, taking part in *de novo* vessel formation [68, 69]. Interestingly, access to the vasculature is also characteristic for neural stem cell niches [69]. These findings support the notion that normal stem cells and CSC share the oxygen dependence.

In the present work the role of Imp2 in GBM CSC was investigated. Experimental evidence show that Imp2 expression is crucial for normal respiratory chain function in GBM CSC and that Imp2 modulates OxPhos also when overexpressed in astrocytes, suggesting that this new function of IGF2 mRNA binding protein is not necessarily cell-specific. Genome wide association studies have shown an important single nucleotide polymorphism in Imp2 gene in patients with type 2 diabetes [54]. This disease can be characterized by defects in insulin responsiveness in skeletal muscle and liver cells and aberrant insulin secretion by pancreatic β cells. Both of these features can be linked to mitochondrial dysfunction, observed as decreased expression of nuclear-encoded genes regulating mitochondrial functions and decreased OxPhos activity [70]. Following the conclusion of the present work, it is plausible that mutations of Imp2 are also interfering with its expression and function in skeletal muscles, liver and pancreas, distorting OxPhos and accounting significantly for the disease phenotype.

Imp2 interactions with OxPhos proteins and mitochondria-related transcripts do not explain the exact mechanism of metabolic control governed by this protein. There are two lines of research that could lead to further characterization of Imp2 function. First, Imp2 could serve as a mitochondrial delivery system. mRNAs bound by Imp2 are all encoded by nuclear genes, yet their protein counterparts are often found in mitochondria. It has been shown that translation of this kind of proteins can occur on the surface of mitochondria, on mitochondria-associated polyribosomes [71]. Imp2 also can be found on the surface of mitochondria. Therefore, isolation of mitochondria-associated polysomes in the presence or absence of Imp2 and quantification of Imp2-bound transcripts on those polysomes could provide results to support mitochondrial transporter function of Imp2. In this model interaction with respiratory complex I proteins could serve as a signal for Imp2 cargo release. However, the proteins of complex I that were bound by Imp2 are all implicated in the early steps of complex assembly. It is plausible that Imp2 serves as a docking molecule for the assembly seed or as a delivery system governing the assembly of complex I. Interestingly, since complex I is the electron entry point for the respiratory chain, its defects can severely affect the whole system, also by impairment of multicomplex assembly. Thus, it could be that Imp2 controls complex I assembly initiation, that provides a signal for further assembly of respiratory chain complexes.

As shown in the above section, Imp2 is highly expressed in glioblastoma and GBM CSC and it is absent or less abundant in low grade gliomas and more importantly it is not expressed in normal brain samples. Only one study aimed at determining Imp2 expression in normal human tissues [72], showing that it is present in gonads. In mouse tissues the highest level of Imp2 expression was observed in the brain [73]. Yet, it is not clear whether Imp2 expression is restricted to cancer cells and stem cells, as it is an oncofetal protein. However, at least in the brain, Imp2 seems to constitute an interesting therapeutical target. Since it is an mRNA binding protein, designing a sequence that could compete with its targets could be a potential approach towards a specific drug design for GBM patients. Further studies of Imp2 role in other cancer and normal stem cell systems would be necessary to evaluate safety of such potential treatment.

Original article

Oxidative phosphorylation controlled by Imp2 is crucial for preserving glioblastoma cancer stem cells

Michalina Janiszewska*[1], Mario-Luca Suvà*[2], Nicolo Riggi[1], Riekelt H. Houtkooper[3], Johan Auwerx[3], Virginie Clément - Schatlo[4], Ivan Radovanovic[4], Esther Rheinbay[2, 5], Paolo Provero[6] and Ivan Stamenkovic[1]

[1]Experimental Pathology
Department of Pathology and Experimental Medicine
CHUV, University of Lausanne, Switzerland
[2]James Homer Wright Pathology Laboratories
Department of Pathology, Massachusetts General Hospital and Harvard Medical School, Boston, Massachusetts, USA

[3]Laboratory for Integrative and Systems Physiology and Nestle Chair in Energy Metabolism (NCEM), Ecole Polytechnique Fédérale de Lausanne, Lausanne, Switzerland
[4]Laboratory of Brain Tumor Biology, Department of Clinical Neurosciences – Neurosurgery, University Hospital of Geneva, Geneva, Switzerland
[5]Bioinformatics Program at Boston University, Boston, Massachusetts, USA
[6]Department of Biochemistry, Molecular Biology and Biotechnology, University of Torino, Torino, Italy
***These authors contributed equally to the work**
Correspondence to Ivan Stamenkovic
Tel: +41 21 314 7136
Fax: +41 21 314 7110
Email: Ivan.Stamenkovic@chuv.ch

Running title: Imp2 in glioblastoma cancer stem cells

Abstract

Cancer stem cells (CSC) occupy the apex of the cellular hierarchy in numerous cancer types, having the capacity for self-renewal and generation of non-tumourigenic progeny. These cells are believed to constitute the driving force of tumour development and progression but neither their energy requirements nor the mechanisms that regulate their energy production are known. Here, we show that the oncofetal insulin-like growth factor 2 mRNA binding protein 2 (IMP2, IGF2BP2) regulates oxidative phosphorylation (OXPHOS) in glioblastoma (GBM) CSC. We provide evidence that IMP2 binds several nuclear-derived mRNAs that encode mitochondrial respiratory chain complex proteins and that it interacts with Complex I (NADH:ubiquinone oxidoreductase) subunits. Depletion of IMP2 in GBM CSC causes a decrease in their oxygen consumption rate and in Complex I activity that results in decreased clonogenicity *in vitro* and tumourigenicity

***in vivo*. Importantly, inhibition of OXPHOS abolishes GBM CSC clonogenicity whereas inhibition of glycolysis has no effect. Our observations suggest that GBM CSC are dependent on OXPHOS but not on glycolysis for their energy production and survival and that IMP2 re-expression provides a key mechanism to ensure OXPHOS maintenance by addressing respiratory chain subunit encoding mRNA to mitochondria.**

Introduction

A growing number of malignancies are recognized to be composed of phenotypically heterogeneous cells that are hierarchically organized and have diverse degrees of differentiating and proliferative capacity (Clevers, 2011). At the apex of the hierarchy are slowly cycling, undifferentiated cells that can self-renew, give rise to proliferating cell subpopulations and reconstitute a phenocopy of the primary tumour upon injection into immunocompromized mice – properties that have earned them the denomination of cancer stem cells (CSC). CSC can be functionally defined based on no more than a handful of properties, including their ability to form spheres *in vitro* under serum-free conditions, initiate tumour formation *in vivo* and display higher resistance to conventional anticancer therapy than their non-spherogenic counterparts (Dean et al., 2005). Yet, numerous key biological properties of these cells that may lead to a better understanding of their behaviour in addition to disclosing their potential therapeutic targetability need to be elucidated.

Because CSC display plasticity that is typically associated with developing tissues, oncofetal proteins may participate in and potentially even determine many of their phenotypic and functional features. The oncofetal protein Imp2 is expressed in the developing mammalian brain and is required for normal embryonic development (Christiansen et al., 2009). Imp2 is an mRNA binding protein that plays an important role in subcellular mRNA localization, translation and stability (Christiansen et al., 2009). Studies on paralogue proteins IMP1 and IMP3 have shown a correlation between their expression and poor outcome in various malignancies, including pancreatic adenocarcinoma, prostate carcinoma, thyroid carcinoma, breast cancer, colon carcinoma, melanoma and ovarian cancer (Dimitriadis et al., 2007; Himoto et al., 2005; Kobel et al., 2007; Yaniv and Yisraeli, 2002), but mechanisms that underlie their functional implication in tumor biology have not been identified so far. Recent evidence suggests that Imp2 is implicated in type 2 diabetes (Christiansen et al., 2009) and in regulating smooth muscle cell adhesion and motility (Boudoukha et al., 2010) but with the exception of its expression in diverse malignancies (Hammer et al., 2005), virtually nothing is

known about its role in cancer. Because of its expression in the developing brain, we chose to address its possible functional role in glioblastoma (GBM) CSC.

Glioblastomas (grade IV astrocytomas) are among the most malignant form of brain tumour with a survival time of approximately one year and notorious resistance to conventional anti-cancer therapy(Louis, 2006). Cells that fulfil the currently accepted functional CSC criteria have been isolated from GBM based on their expression of diverse cell surface markers, including CD133 (Singh et al., 2004), SSEA1 (Son et al., 2009) and CD44 (Anido et al., 2010). Glioblastoma thus provides a suitable solid tumor model to investigate CSC properties. We therefore addressed IMP2 expression, the repertoire of its target mRNAs and its functional relevance in GBM.

Results and discussion

Immunohistochemical staining of normal brain tissue and a panel of gliomas of varying grades revealed that Imp2 is absent in normal brain and grade II and III gliomas (Fig.1A), whereas 40 out of 51 GBM samples were Imp2-positive (data not shown). These observations were confirmed by microarray analysis of Imp2 expression in an independent dataset of 153 gliomas of different grades and 23 normal samples (Sun et al., 2006) (Fig. 1B). Quantitative real-time PCR (Q-PCR) on extracts from primary GBM cells sorted for expression of the CSC-associated marker CD133 showed higher Imp2 expression in CD133+ than in CD133- GBM cells (Fig.1C, left). To investigate the role of Imp2 in GBM CSC *in vitro*, we used primary human GBM cells derived from three independent tumours (BT1-3) cultured as spheres in serum-free conditions. All three isolates have been shown to form tumours *in vivo* that are a phenocopy of the tumour they were derived from (Suvà et al., 2009). Consistent with our Q-PCR data, a high level of Imp2 expression was observed in gliospheres, as assessed by immunofluorescence (Fig.1C, right).

To begin to address its putative role in GBM CSC, Imp2 ribonucleoprotein (RNP) complexes were immunoprecipitated and Imp2-bound mRNA transcripts were analyzed on Affymetrix microarrays. In parallel, pull-down experiments using anti-Imp2 antibody were performed to identify Imp2-bound proteins. Among 400 transcripts that were bound by Imp2, significant overrepresentation of genes implicated in mitochondrial function and OXPHOS was found (Fig. 2A and 2B, Supplemental Table 1). Implication of Imp2 in OXPHOS was supported by the identification of several subunits of Complex I of the mitochondrial respiratory chain in the pulldown material (Fig. 2C). Complex I catalyzes electron transfer from NADH to ubiquinone and constitutes the main entry point of electrons into the respiratory chain (Carroll

et al., 2006; Murray et al., 2003). Two subunits, NADH dehydrogenase (ubiquinone) iron-sulphur protein 3 (NDUFS3) and iron sulphur protein 7 (NDUFS7) that form part of the peripheral arm of the complex (Fernandez-Vizarra et al., 2009), as well as NADH dehydrogenase (ubiquinone) 1 alpha complex assembly factor 3 (NDUF3) were identified in the Imp2 pulldown. Interaction between Imp2 and NDUFS3 was validated by immunoprecipitation and Western blot analysis (Fig. 2D).

To assess the functional relevance of Imp2 expression in GBM CSC, stable repression of Imp2 transcripts using specific shRNA sequences was performed. Imp2 depletion resulted in a decrease in NDUFS3 protein (Fig. 3A) and Imp2-bound transcript (Fig. 3B) levels. Cells depleted of Imp2 had markedly impaired ability to form spheres in clonogenic assays *in vitro* (Fig. 3C) and their capability to form tumours *in vivo* was also compromised (Fig. 3D). Expression of Imp2 shRNA altered the morphology of the spheres (Fig. 5), due, at least in part, to increased cell death as assessed by propidium iodide staining (Supplemental Fig. 1A). Interestingly, the observed cell death was not apoptotic, as no increase in caspase 3 activation (Supplemental Fig. 1B) and no difference in Annexin V staining between Imp2-expressing and Imp2-depleted cells (data not shown) were observed. It had been shown previously that cells bearing mutations that impair the mitochondrial respiratory chain alter their response to pro-apoptotic stimuli (Kwong et al., 2007). Notably, cells devoid of mitochondrial DNA or bearing mutations resulting in a global loss of respiratory chain complexes were found to be resistant to staurosporin (STS)- and thapsigargin (TG)-induced apoptosis (Kwong et al., 2007). Similarly, and in contrast to control shRNA expressing cells, Imp2-depleted cells did not undergo apoptosis in response to STS or TG (Supplemental Fig. 1C) leading to the conclusion that Imp2 may play a role in sustaining OXPHOS in CSC.

To explore this possibility, we investigated the effect of Imp2 depletion on mitochondrial activity. MitoTracker Red staining that provides an indication of mitochondrial activity was significantly decreased in Imp2-depleted cells (Fig. 4A). However, based on the observation that cell death was increased among Imp-2-deficient cell populations, decreased mitochondrial activity could simply reflect lower overall numbers of viable cells with active mitochondria. To address possible changes in mitochondrial activity following Imp2 depletion, oxygen consumption and extracellular acidification rate measurements were made in equal numbers of GBM CSC depleted or not of Imp2. Cells expressing Imp2 shRNA displayed a significantly decreased oxygen consumption rate (Fig. 4B), but an unaltered extracellular

acidification rate (data not shown). Because the assay was performed on live cells, equal viable cell seeding could be verified by Calcein AM staining (Fig. 4C) following the measurements. Inhibition of respiratory Complex I by addition of rotenone to the cell culture medium during the measurement decreased the oxygen consumption rate of control shRNA expressing cells to the level measured in Imp2 deficient cells (Fig. 4D), supporting the notion that the difference in oxygen consumption rate was due to a defect in OXPHOS. Next, we excluded impairment of mitochondrial biogenesis as an explanation for the oxygen consumption decrease. Q-PCR for mitochondrial DNA content showed that cells depleted of Imp2 had higher mitochondrial numbers (Fig. 4E), consistent with accumulation of functionally impaired mitochondria that is observed in several mitochondrial diseases and that may reflect a compensatory event (Johannsen and Ravussin, 2009).

To further address the relationship between Imp2 and mitochondrial respiration, the effect of Imp2 introduction was assessed in astrocytes in which its expression is undetectable by immunocytochemistry and barely detected at the transcript level. Overexpression of Imp2 in the human astrocyte cell line SVGp12 resulted in increased Imp2 interacting protein levels, augmented mitochondrial function, as assessed by MitoTracker Red staining and a higher oxygen consumption rate (Supplemental Fig. 2). To determine whether the observed effects could be related to changes in Complex I activity, we performed a Blue Native PAGE (BN-PAGE) that allowed us to separate mitochondrial respiratory chain complexes and to perform in-gel measurements of their enzymatic activity (Nijtmans et al., 2002). Mitochondrial extracts from GBM CSC stably transfected with Imp2 shRNA showed a marked decrease in complex I activity (Fig. 4F).

The mechanism whereby Imp2 controls mitochondrial metabolism could involve stabilization of its target mRNAs and/or their subcellular localization to the vicinity of mitochondria. To determine whether degradation of Imp2 target mRNAs depends on its expression, cells overexpressing or depleted of Imp2 were treated with actinomycin D to block mRNA polymerization. Degradation of a panel of target transcripts was then assessed at several time points for a total of 12 hours (Supplemental Fig. 3A). Although the expression level of the target RNAs was dependent on that of Imp2, the slope of the decay curve was not altered, suggesting that Imp2 does not play a major role in its target mRNA stability. Next, Imp2 localisation was assessed by Western blot analysis of subcellular GBM CSC fractions using anti-Imp2 antibody. Imp2 was found in the cytoplasm as well as in intact mitochondria, where

NDUFS3 is also located (Supplemental Fig. 3B, lane 2). Proteinase K treatment of mitochondria abolished Imp2 detection consistent with its localization on the mitochondrial surface (Supplemental Fig. 3B, lane 3). Partial degradation of NDUFS3 observed following proteinase K treatment suggests that a fraction of its cellular content is localized on the mitochondrial surface where interaction with Imp2 may occur. Together, these observations suggest at least two candidate mechanisms that may underlie Imp2-dependent OXPHOS regulation. First, Imp2 may serve to deliver nuclear transcripts that encode mitochondrial respiratory chain complex subunits to the mitochondrial surface where the corresponding protein synthesis occurs. Complex I subunits with which Imp2 interacts may serve as a mitochondrial surface docking platform for the corresponding ribonucleoprotein particles. Second, Imp2 interaction with Complex I subunits may influence their stability, assembly and possible formation of supercomplexes with Complex III and IV that appear to be necessary for respiratory activity (Fernandez-Vizarra et al., 2009)

Our observations provide evidence that GBM CSC require an intact respiratory chain to sustain their tumourigenic potential. To address the relative importance of oxidative phosphorylation and anaerobic glycolysis in GBM CSC we used inhibitors of each pathway, including rotenone, which blocks Complex I activity, and oxamic acid, which abrogates lactate dehydrogenase (LDH), respectively. Rotenone treatment recapitulated the effect of Imp2 shRNA on GBM CSC with disruption of sphere morphology and abrogation of clonogenicity (Fig. 5). By contrast, oxamic acid increased the number of spheres in culture (although this effect was not significant) as shown by post-treatment clonogenic assays. The same assays were then performed on differentiated primary GBM cells obtained by culturing CSC in serum-containing medium, instead of "spherogenic" medium (Singh et al., 2004). Following treatment with rotenone, adherent GBM cells underwent transient attenuation of proliferation from which they rapidly recovered (Supplemental Fig. 4A). By contrast, viable cell counts after oxamic acid treatment revealed a 40% decrease in cell number in comparison to control cells (Supplemental Fig. 4B). Comparison of oxygen consumption rates between astrocytes, and CSC that were allowed to adhere to culture plates or maintained as spheres expressing or not Imp2 shRNA, revealed significant differences in metabolic activity (Supplemental Fig. 4C). Remarkably, CSC maintained as spheres that we have shown to rely heavily on mitochondrial respiration, had a far lower oxygen consumption rate than either primary astrocytes or adherent GBM cells.

Bioenergetic reprogramming constitutes part of the profound alterations induced by transformation and the ensuing changes in growth patterns and augmented anabolism impose increased energy requirements on transformed cells compared to their normal counterparts (Hanahan and Weinberg, 2011). The longstanding view, first proposed by Warburg, is that these requirements are primarily fulfilled by glycolysis even in the presence of adequate oxygen supply (Vander Heiden et al., 2009). Glycolysis provides rapid but inefficient energy production, generating 2-4 moles of ATP per mole of glucose. However, glucose along with glutamine is the major source of carbon, free energy and reducing equivalents required to support cell growth and division. Thus, a substantial portion of glucose is likely to be used to generate macromolecular precursors of fatty acid, non-essential amino acid and nucleotide synthesis in proliferating cells. Nevertheless, glycolysis is not a major energy source in all cancer cells (Jose et al., 2010) and those that have not sustained major mitochondrial damage or corresponding DNA mutations, may alternate between OXPHOS and glycolysis depending on their state and microenvironment. Slowly proliferating cells, such as CSC, may utilize the more efficient OXPHOS pathway that yields 36 moles of ATP per mole of glucose. Oxygen supply, required for OXPHOS, is probably more readily available for GBM CSC than for more differentiated GBM cells based on the observations that GBM CSC reside in the proximity of blood vessels (Calabrese et al., 2007) and that they may even generate tumour endothelium (Ricci-Vitiani et al., 2010; Wang et al., 2010). As CSC progeny proliferates, increased anabolic requirements and/or genetic mutations that inactivate mitochondria could force the cells to switch to a predominantly glycolytic metabolism. Hypoxic tumour regions with diminished nutrient supply may further select for survival of cancer cells that can efficiently switch to glycolysis (Rodriguez-Enriquez et al., 2010). It is therefore plausible that the hierarchical cellular organization within a tumour is also reflected in metabolic differences between cancer cells.

Our study provides the novel observations that an mRNA binding oncofetal protein, Imp2, controls OXPHOS in GBM CSC and that OXPHOS is essential for CSC survival, clonogenicity and tumour initiating potential. In addition to providing new insight into mechanisms of energy production in GBM CSC, these findings may have important clinical implications as Imp2 is not expressed in normal brain and its inhibitors may provide an attractive therapeutic option in glioblastoma.

Materials and methods

Chemical compounds and treatments

For the apoptosis induction assay BT cells were treated with 1μM staurosporin (STS, kindly provided by Phil Shaw) or 1μM thapsigargin (TG, Tocris Bioscience) for 6h and 24h, respectively. Treatment duration was chosen to induce minimal apoptotic response.

For mRNA degradation studies 10μg/ml actinomycin D (Sigma) was added to cell growth medium. RNA was collected after 0, 4, 8 and 12h of treatment.

Inhibition of OXPHOS was achieved by 1μM rotenone (Sigma). Lactate dehydrogenase inhibitor oxamic acid was used at 25mM to block glycolysis. Both treatments were applied for 72h.

Tumor samples, CSC culture, adherent primary cultures and clonogenic assay

Experimental procedures were performed as previously described (Suvà et al., 2009).

Imp2 knockdown and retroviral infection

The shRNA sequences targeting Imp2 were: sh1 – sense strand: 5' GATCCACCAAACTAGCCGAAGAGATTCAAGAGATCTCTTCGGCTAGTTTGGTTTT TTTACGCGTG3', antisense strand: 5'AATTCACGCGTAAAAAAACCAAACTAGCCGA AGAGATCTCTTGAATCTCTTCGGCTAGTTTGGTG3'; sh2 – sense strand: 5'GATCCGCGGAAAGAACCATCACTGTTTCAAGAGAACAGTGATGGTTCTTTCCGT TTTTTACGCGTG3', antisense strand: 5'AATTCACGCGTAAAAAACGGAAAGAACCA TCACTGTTCTCTTGAAACAGTGATGGTTCTTTCCGCG3'. Sense and antisense oligonucleotides were annealed to form duplexes and inserted into the pSIREN-Retro Q retroviral vector (BD Biosciences Clontech), according to the manufacturer's recommendations. Imp2 or control shRNA plasmids were transfected into GP2 packaging cells to produce the virus used to infect target gliomaspheres. Viral supernatant was concentrated by ultracentrifugation using a SW28 rotor (Beckman Coulter) at 19,500 rpm for 90 min. Concentrated virus was added to dissociated spheres. Forty-eight hours later, cells were selected for puromycin (2 μg/ml) resistance for 5 days. The efficiency of the Imp2 knockdown was verified by real-time quantitative PCR and Western blot analysis.

Imp2 overexpression

The PCR product generated with following primers: Fwd 5'GAAGATCTTCCCAC CATGATGAACAAGCTTTACATC3', Rev 5'CGGAATTCTCACTTGCTGCGCTGTGA GGCGACT3' on GBM CSC genomic DNA was cloned into pMSCV_puro vector (Clonetech). Human astrocyte cell line SVGp12 was infected with pMSCV_Imp2 or empty vector containing virus according to the standard protocol. Cells were selected for puromycin (2 μg/ml) resistance for 7 days.

Nonobese diabetic–severe combined immunodeficient mice xenotransplantation and survival analysis

The *in vivo* experiments were conducted as described previously (Suvà et al., 2009). Six mice were used per condition. Survival analysis significance was calculated with log-rank test.

Immunohistochemistry

Paraffin-embedded sections of gliomas and normal brain were stained with mouse anti-human Imp2 (1:50 Dilution, Abcam). HRP staining was performed using biotin-conjugated rabbit anti-mouse IgG (Vector Laboratories) and revealed with a DAKO DAB Kit (DAKO).

Immunofluorescence

Gliospheres or adherent GBM cells were fixed with 4%PFA, washed, permeabilized with 3% Triton-X100, incubated with anti-Imp2 antibody (1:100, 0.5μg/ml, Abcam) for 30min, followed by donkey anti-mouse-Alexa488 (1 :1300, Molecular Probes) and mounted in 1 :1000 DAPI in mounting medium (ThermoShandon). Antibody specificity was compared to the isotype-matched control antibody. Images were acquired with Leica SP5 AOBS confocal microscope at the Imaging Core Facility of the University of Lausanne. The acquisition was performed in sequential mode to avoid dye crosstalk. 3D reconstruction of sphere staining was done with Imaris software.

Q-PCR

The procedure was performed as described previously (Suvà et al., 2009). For normalization, 18S probe was used as the endogenous control. Q-PCR primers are presented in the table.

Gene name	Fwd primer	Rev primer
Imp2	AACAGGACTGTCCGTGCTAT	CTCTGGATAAGAGTGATGAT
GPR160	CCAGCCATCTACCAAAGC	ATCCTGATAGCCTGTACC
POLR1D	GAAGACCTCAATGGCTGAAG	AGGATGGGTCGTAGTGTAAC
TAF9B	CCCTTTGCCACTGATTAAGC	TTTGGGACAGACACCGTTTG
Nxt2	AGGTAGTGACGCCGACACTG	CCTGGTTAGTGCCCGTCTTC
HMGA1	AAGGAGCCCAGCGAAGTGCCAAC	AGCCTTGTCCAGGAGGGCATGTG
DPH3	ATGACGAGGACTCGGAGAC	GGGCTGGGACTGTTTCTCCACAC
NDUFAF4	TCCTGCGAGAGCAGATTAGTC	CGGCAATCTGAATTCCTTCGG
COX7b	GAAGCGAATTGGCACCAAAG	GTGGCTCCACTAGCTAATAC
COX7c	GTGCCGCCATTTCATCTGTC	AGGGTGTAGCAAATGCAGATCC
COX16	GAACAAGACTCTCGGCTATGG	TTGGAGGAGGTCAGGATCTTC
CYB5b	AAACCTGCCTCAGTAGAGTC	CAGGCTCAAACGATAGGTTC
MRLQ	TCTCTTGCGTCTGGCATTG	ATTGTGCGGATGTGGCTTC

To determine mitochondrial content, Q-PCR was performed on DNA extracts using 18S primers (Fwd 5' TAGAGGGACAAGTGGCGTTC3', Rev 5' CGCTGAGCCAGTCAGTGT 3') for nuclear DNA and 16S primers (Fwd 5' CACCCAAGAACAGGGTTTGT3', Rev 5' TGGCCATGGGTATGTTGTTAA3') for mitochondrial DNA and the ratio of the two was calculated.

Western blot

Western blotting was performed according to standard procedures. The following antibodies were used: anti-Imp2 (0.5µg/ml, Abcam), anti-NDUFS3 (0.5µg/ml, Abcam), anti-PARP (0.5µg/ml, Cell Signalling), anti-caspase 3 p20 (0.2µg/ml, Santa Cruz), anti-β-actin (1.65µg/ml, Sigma), anti-α-tubulin (0.025µg/ml, Calbiochem). Secondary antibodies were horseradish peroxidase (HRP)–conjugated goat anti-mouse (GE Healthcare), mouse anti-rabbit (DAKO) and rabbit anti-goat (DAKO) antibodies.

Propidium iodide staining and cell cycle analysis

Cells were resuspended in 10ng/ml propidium iodide with 1% IGEPAL, vortexed, incubated overnight at 4°C and analyzed by FACS.

Intact mitochondria isolation and proteinase K treatment

Intact mitochondria were isolated from 20 x 10^6 GBM CSC with Mitochondria Isolation Kit for Cultured Cells (Pierce). To remove proteins from the mitochondrial surface, mitochondrial pellets were resuspended in buffer C (Mitochondria Isolation Kit for Cultured Cells, Pierce) and treated with 50µg/ml proteinase K (Sigma) for 30min on ice and spun down at 10000xg for 10min.

RIP-CHIP assay

30 x 10^6 BT cells were used per experiment. Imp2-bound RNA immunoprecipitation was performed according to the RiboCluster Profiler RIP-Assay Kit protocole (MBL Ribonomics). Eluted RNA was anaylzed at the DNA Array Facility Lausanne using Affymetrics Arrays. RIP-CHIP results generated from 3 different primary cultures were compared. Probe sets showing a false discovery rate < 0.05 and logarithmic fold changes > 2 in all three samples were subjected to further analysis. Gene Onthology annotations obtained for those probes were considered as overrepresented when the P value of exact one-tailed Fisher test was < 0.00005.

Pull-down assay

80 x 10^6 cells were collected in PBS with protein inhibitors, centrifuged, resuspended in 5 volumes of the RIP-Assay lysis buffer (without addition of DTT) and sonicated for 10s. The lysate was centrifuged at 3500rpm for 5min at 4°C. Agarose protein-A beads (GE Healthcare), previously washed with wash buffer from the RIP-Assay kit, without DTT, were added to the supernatants and discarded after 2h of pre-clearing. Incubation with 20µg of anti-Imp2 or isotype matched control antibody was performed overnight at 4°C, and incubation with the beads for 4h. The beads were then washed 4 times with wash buffer. Mass-spectrometry analysis was performed at the *Protein Analysis Facility of Faculty of Biology and Medecine, University of Lausanne.*

Mitotracker assay

Cells were washed twice with PBS, resuspended in pre-warmed medium containing 250nM MitoTracker Red CM-H2XRos (Molecular Probes) or DMSO and incubated for 30min at 37°C. After two washes with PBS, cells were resuspended in PBS and analyzed by FACS.

OCR/ECAR measurement

20,000 to 50,000 cells per well were seeded in XF24 cell culture microplates (Seahorse Bioscience). For each cell type 5 replicates were made. Measurements for spherogenic cells were made immediately after sphere disruption and viable cell counting (Trypan blue exclusion) and following the assay, cell viability was verified (Calcein AM staining (1:200, 2mg/ml, Calbiochem) analyzed by FACS). For adherent cells, measurements were made 12-16h after seeding, and absence of difference in cell proliferation was verified using a Cell Proliferation ELISA BrdU colorimetric assay (Roche).

Blue Native PAGE and in-gel activity assay

The mitochondrial extracts preparation, Blue Native gel electrophoresis and in-gel activity for respiratory complex I were performed as described (Nijtmans et al., 2002).

Statistical methods

Microarray gene expression data for non-malignant brain and different gliomas were obtained from Sun et al (Sun et al., 2006) (GEO accession GSE4290). Data were normalized with RMA and probes corresponding to the same gene were collapsed to the maximum value using the GenePattern software package (Reich et al., 2006). T-test p-values for sample comparisons were calculated using the R statistical software package (Team, 2010).

P values were calculated with Graph Pad Prism 5 software, using statistical tests indicated in figure legends.

Acknowledgments

We thank Keith Harshman from Genomic Technologies Facility, Center for Integrative Genomics, *Faculty of Biology and Medecine*, University of Lausanne, *Switzerland* for performing the microarray experiment; Manfredo Quadroni from Protein Analysis Facility, Center for Integrative Genomics, *Faculty of Biology and Medicine, University of Lausanne, Switzerland* for the mass-spectrometry analysis. We also thank Whitney Quong, Claudio De Vito, Karine Baumer and Carlo Fusco for technical assistance and discussions and Sylviane Trepey for immunohistochemistry. P.P. acknowledges funding from the Italian Association for Cancer Research (AIRC). R.H.H. was supported by a Rubicon fellowship from the Netherlands Organization for Scientific Research (NWO). The work in the Auwerx laboratory was supported by grants of the Ecole Polytechnique Fédérale de Lausanne, Swiss National

Science Foundation, NIH (DK59820), the Velux Stiftung, and the European Research Council Ideas programme (Sirtuins; ERC-2008-AdG23118). The authors thank all the members of the Auwerx lab for inspiring discussions.

References

Anido, J., A. Sáez-Borderías, A. Gonzàlez-Juncà, L. Rodón, G. Folch, M.A. Carmona, R.M. Prieto-Sánchez, I. Barba, E. Martínez-Sáez, L. Prudkin, I. Cuartas, C. Raventós, F. Martínez-Ricarte, M.A. Poca, D. García-Dorado, M.M. Lahn, J.M. Yingling, J. Rodón, J. Sahuquillo, J. Baselga, and J. Seoane. 2010. TGF-² Receptor Inhibitors Target the CD44high/Id1high Glioma-Initiating Cell Population in Human Glioblastoma. *Cancer Cell*. 18:655-668.

Boudoukha, S., S. Cuvellier, and A. Polesskaya. 2010. Role of the RNA-binding protein IMP-2 in muscle cell motility. *Mol Cell Biol*. 30:5710-5725.

Calabrese, C., H. Poppleton, M. Kocak, T.L. Hogg, C. Fuller, B. Hamner, E.Y. Oh, M.W. Gaber, D. Finklestein, M. Allen, A. Frank, I.T. Bayazitov, S.S. Zakharenko, A. Gajjar, A. Davidoff, and R.J. Gilbertson. 2007. A perivascular niche for brain tumor stem cells. *Cancer Cell*. 11:69-82.

Carroll, J., I.M. Fearnley, J.M. Skehel, R.J. Shannon, J. Hirst, and J.E. Walker. 2006. Bovine complex I is a complex of 45 different subunits. *J Biol Chem*. 281:32724-32727.

Christiansen, J., A.M. Kolte, T.v.O. Hansen, and F.C. Nielsen. 2009. IGF2 mRNA-binding protein 2: biological function and putative role in type 2 diabetes. *J Mol Endocrinol*. 43:187-195.

Clevers, H. 2011. The cancer stem cell: premises, promises and challenges. *Nat Med*. 17:313-319.

Dean, M., T. Fojo, and S. Bates. 2005. Tumour stem cells and drug resistance. *Nat Rev Cancer*. 5:275-284.

Dimitriadis, E., T. Trangas, S. Milatos, P.G. Foukas, I. Gioulbasanis, N. Courtis, F.C. Nielsen, N. Pandis, U. Dafni, G. Bardi, and P. Ioannidis. 2007. Expression of oncofetal RNA-binding protein CRD-BP/IMP1 predicts clinical outcome in colon cancer. *Int J Cancer*. 121:486-494.

Fernandez-Vizarra, E., V. Tiranti, and M. Zeviani. 2009. Assembly of the oxidative phosphorylation system in humans: what we have learned by studying its defects. *Biochim Biophys Acta*. 1793:200-211.

Hammer, N.A., T.O. Hansen, A.G. Byskov, E. Rajpert-De Meyts, M.L. Grondahl, H.E. Bredkjaer, U.M. Wewer, J. Christiansen, and F.C. Nielsen. 2005. Expression of IGF-II mRNA-binding proteins (IMPs) in gonads and testicular cancer. *Reproduction*. 130:203-212.

Hanahan, D., and Robert A. Weinberg. 2011. Hallmarks of Cancer: The Next Generation. *Cell*. 144:646-674.

Himoto, T., S. Kuriyama, J.Y. Zhang, E.K. Chan, Y. Kimura, T. Masaki, N. Uchida, M. Nishioka, and E.M. Tan. 2005. Analyses of autoantibodies against tumor-associated antigens in patients with hepatocellular carcinoma. *Int J Oncol*. 27:1079-1085.

Johannsen, D.L., and E. Ravussin. 2009. The role of mitochondria in health and disease. *Current Opinion in Pharmacology*. 9:780-786.

Jose, C., N. Bellance, and R. Rossignol. 2010. Choosing between glycolysis and oxidative phosphorylation: A tumor's dilemma? *Biochim Biophys Acta*.

Kobel, M., D. Weidensdorfer, C. Reinke, M. Lederer, W.D. Schmitt, K. Zeng, C. Thomssen, S. Hauptmann, and S. Huttelmaier. 2007. Expression of the RNA-binding protein IMP1 correlates with poor prognosis in ovarian carcinoma. *Oncogene*. 26:7584-7589.

Kwong, J.Q., M.S. Henning, A.A. Starkov, and G. Manfredi. 2007. The mitochondrial respiratory chain is a modulator of apoptosis. *The Journal of Cell Biology*. 179:1163-1177.

Louis, D.N. 2006. Molecular pathology of malignant gliomas. *Annu Rev Pathol*. 1:97-117.
Murray, J., B. Zhang, S.W. Taylor, D. Oglesbee, E. Fahy, M.F. Marusich, S.S. Ghosh, and R.A. Capaldi. 2003. The subunit composition of the human NADH dehydrogenase obtained by rapid one-step immunopurification. *J Biol Chem*. 278:13619-13622.
Nijtmans, L.G., N.S. Henderson, and I.J. Holt. 2002. Blue Native electrophoresis to study mitochondrial and other protein complexes. *Methods*. 26:327-334.
Reich, M., T. Liefeld, J. Gould, J. Lerner, P. Tamayo, and J.P. Mesirov. 2006. GenePattern 2.0. *Nat Genet*. 38:500-501.
Ricci-Vitiani, L., R. Pallini, M. Biffoni, M. Todaro, G. Invernici, T. Cenci, G. Maira, E.A. Parati, G. Stassi, L.M. Larocca, and R. De Maria. 2010. Tumour vascularization via endothelial differentiation of glioblastoma stem-like cells. *Nature*. 468:824-828.
Rodriguez-Enriquez, S., L. Carreno-Fuentes, J.C. Gallardo-Perez, E. Saavedra, H. Quezada, A. Vega, A. Marin-Hernandez, V. Olin-Sandoval, M.E. Torres-Marquez, and R. Moreno-Sanchez. 2010. Oxidative phosphorylation is impaired by prolonged hypoxia in breast and possibly in cervix carcinoma. *Int J Biochem Cell Biol*. 42:1744-1751.
Singh, S.K., C. Hawkins, I.D. Clarke, J.A. Squire, J. Bayani, T. Hide, R.M. Henkelman, M.D. Cusimano, and P.B. Dirks. 2004. Identification of human brain tumour initiating cells. *Nature*. 432:396-401.
Son, M.J., K. Woolard, D.-H. Nam, J. Lee, and H.A. Fine. 2009. SSEA-1 Is an Enrichment Marker for Tumor-Initiating Cells in Human Glioblastoma. *Cell Stem Cell*. 4:440-452.
Sun, L., A.-M. Hui, Q. Su, A. Vortmeyer, Y. Kotliarov, S. Pastorino, A. Passaniti, J. Menon, J. Walling, R. Bailey, M. Rosenblum, T. Mikkelsen, and H.A. Fine. 2006. Neuronal and glioma-derived stem cell factor induces angiogenesis within the brain. *Cancer cell*. 9:287-300.
Suvà, M.-L., N. Riggi, M. Janiszewska, I. Radovanovic, P. Provero, J.-C. Stehle, K. Baumer, M.-A. Le Bitoux, D. Marino, L. Cironi, V.E. Marquez, V. Clément, and I. Stamenkovic. 2009. EZH2 Is Essential for Glioblastoma Cancer Stem Cell Maintenance. *Cancer Res*. 69:9211-9218.
Team, R.C. 2010. R : A Language and Environment for Statistical Computing. . *Reference Index Version 2111* 1:3 - 900051
Vander Heiden, M.G., L.C. Cantley, and C.B. Thompson. 2009. Understanding the Warburg Effect: The Metabolic Requirements of Cell Proliferation. *Science*. 324:1029-1033.
Wang, R., K. Chadalavada, J. Wilshire, U. Kowalik, K.E. Hovinga, A. Geber, B. Fligelman, M. Leversha, C. Brennan, and V. Tabar. 2010. Glioblastoma stem-like cells give rise to tumour endothelium. *Nature*. 468:829-833.
Yaniv, K., and J.K. Yisraeli. 2002. The involvement of a conserved family of RNA binding proteins in embryonic development and carcinogenesis. *Gene*. 287:49-54.

Figure legends

Figure 1. *Imp2 expression in GBM* ; A - immunohistochemical staining of paraffin sections shows lack of Imp2 expression in normal brain and low grade gliomas and a spectrum of positive staining in GBM ; B — Imp2 expression across gliomas of different grade in an independent data set (Sun et al) ; t-test P values : GBM vs normal: p=9.678e-11; GBM vs grade II/III oligodendroglioma: p =0.006351; GBM vs grade II/III astrocytoma: p =4.310e-05; C – Imp2 expression is high in GBM CSC; Q-PCR for Imp2 in GBM CD133+ CSC (left panel, results for two independent cell batches are shown); immunofluorescence staining of CSC spheroid (3D reconstruction, middle panel) compared to differentiated cancer cells shows high Imp2 expression levels in cancer stem cells (right panel) ; green immunofluorescence: Imp2 staining, white: Imp2 channel 3D reconstruction (signal above threshold), blue: DAPI; two independent staining were performed;

Figure 2. *mRNA and proteins bound by Imp2 suggest a functional role in mitochondrial processes*; A – specificity of RIP assay is presented by the heat map comparing transcripts obtained with anti-Imp2 and isotype matched ctrl antibody immunoprecipitation; results for three batches of primary GBM cultures in spherogenic conditions are shown; B - gene ontology analysis of Imp2-bound RNA shows overrepresentation of mitochondrial processes; GO term was considered enriched if the nominal P of the exact one-tailed Fisher test was less than 10^{-5}; the length of the bar for each term is proportional to the number of bound mRNAs annotated to the term; the shaded part of the bar represents the number of annotated mRNAs expected by chance; C – mass-spectrometry analysis of Imp2-bound proteins suggests an interaction with mitochondrial respiratory complex I proteins ; D - immunoperecipitation of Imp2 (left panel) followed by Western blotting using an anti-NDUFS3 antibody and immunoprecipitation of NDUFS3 (right panel) followed by Western blotting using an anti-Imp2 antibody confirm the interaction between the two proteins;

Figure 3. *Effects of Imp2 knock-down*; A – Imp2 was efficiently silenced in GBM CSC stably expressing two different shRNAs; Imp2 depletion also decreased NDUFS3 protein levels; B – Imp2 knock-down decreases mRNA levels of Imp-2 bound transcripts; Q-PCR for two batches of GBM CSC (black and white bars) are shown; C – Stable Imp2 shRNA expression impairs sphere formation in three batches of GBM CSC (BT-1, BT-2 and BT-3; * - P value 0.0227, ** - P value 0.0015, ***- P value 0.0008, unpaired two-tailed t-test); error bars represent standard deviations; D – Imp2 shRNA expression diminishes GBM CSC tumor forming capacity; the experiment was repeated in three independent batches of cells (circles, squares and triangles); 6 animals were used per condition; since tumor formation by different

BTs varied over time, a timescale of the experiment is presented (with the final time point as 100); the differences between Imp2 and ctrl shRNA expressing cells for each cell batch are significant (Log-rank (Mantel-Cox) test P value for BT-1 is 0.0088, BT-2 is 0.0036, BT-3 is 0.0003);

Figure 4. *Imp2 depletion affects oxidative respiration in GBM CSC*; A – MitoTracker Red staining of active mitochondria decreases in cells depleted of Imp2; representative graphs of 3 experiments with independent cell batches are shown; B – diminished oxygen consumption rate (OCR) is caused by Imp2 shRNA expression in two cell batches (BT-1 and BT-2); **** - P value < 0.0001 (paired two-tailed t-test); error bars represent standard deviation; C - Calcein AM staining was performed immediately after OCR measurement to ensure equal seeding of viable cells for the oxygen consumption measurement; D – 1μM rotenone injection decreases OCR of ctrl cells to a level comparable to that measured in Imp2 depleted cells; **** - P value < 0.0001, ns – not significant (two-way ANOVA with Bonferroni's multiple comparison test); error bars represent standard deviation; representative of two experiments; E - cells depleted of Imp2 accumulate mitochondria; Q-PCR comparison of mitochondrial (16S) to nuclear (18S) DNA content; bars represent mean of two independent experiments on GBM CSC; error bars represent standard deviation; representative of two experiments; F – respiratory complex I activity is lowered by Imp2 knock-down, as shown by Blue Native PAGE and in-gel activity assay; 40μg or 100μg of the mitochondrial extracts were loaded on the gel; representative of three experiments;

Figure 5. *Inhibition of oxidative phosphorylation impairs clonogenicity and survival of GBM CSC*; silencing of Imp2 affects GBM CSC sphere morphology in the same way as inhibition of oxidative phosphorylation with 1μM rotenone treatment (left panel); the clonogenic potential is diminished by Imp2 shRNA expression (Fig. 2) and by rotenone treatment (upper right panel; ** - P value 0.0024, unpaired two-tailed t-test); anaerobic glycolysis inhibition by 25mM oxamic acid does not significantly affect the clonogenic potential of GBM CSC; representative results for one out of three independent cell batches are shown; error bars represent the standard deviation;

Supplemental material

Supplemental Figure 1. *Imp2 knock-down induces non-apoptotic cell death*; A – cell cycle analysis (propidium iodide incorporation analyzed by FACS) shows a decrease in actively cycling cells and an increase in the amount of dead cells in the Imp2 shRNA expressing population; representative of two experiments; B – Imp2 knock-down does not induce apoptosis as caspase 3 cleavage is not enhanced by Western blot analysis; representative of two experiments; C – Imp2 depleted cells are resistant to inducers of apoptosis: apoptosis induction by treatment with 1μM staurosporin (STS) or 1μM thapsigargin (TG) for 6h or 24h, respectively; Western blots using anti-PARP and anti-caspase 3 p20 show weak induction of apoptosis in cells expressing ctrl shRNA but no effect of the drugs on Imp2 depleted cells; representative of two experiments;

Supplemental Figure 2. *Imp2 overexpression in human astrocytes;* A – Western blot analysis of extracts from the SVGp12 human astrocyte cell line expressing pMSCV_Imp2 or ctrl (empty) vector; representative of two experiments; B – MitoTracker Red staining of active mitochondria is increased in SVGp12 cells overexpressing Imp2; representative of three experiments;C – overexpression of Imp2 increases oxygen consumption rate; *** - P value 0.0002 (paired two-tailed t-test); error bars represent standard deviation; the effect of cell proliferation on the OCR was excluded by BrdU incorporation assay (data not shown); representative of three experiments;

Supplemental Figure 3. *Imp2 could provide mRNA delivery system for mitochondria*; A – degradation of Imp2-bound transcripts was measured after 0, 4, 8 and 12h after actinomycin D addition by Q-PCR; the lines represent linear regression; the slopes of the linear regression are not significantly different between Imp2 expressing and depleted cells; representative of 15 transcripts tested; B – Imp2 localizes at the surface of mitochondria; subcellular fractionation: CYT – cytosolic fraction, MT – isolated mitochondria; Western blot for Imp2 and NDUFS3 shows disappearance of Imp2 band upon proteinase K treatment of the intact mitochondria; representative of two experiments;

Supplemental Figure 4. *GBM CSC after differentiation in serum are less sensitive to inhibition of oxidative phosphorylation but more sensitive to glycolysis blockade*; A – GBM CSC cultured in medium containing serum acquire an adherent phenotype and are less sensitive to rotenone treatment than their spherogenic counterparts; left – adherent BT cells treated with DMSO; right - adherent BT cells treated with rotenone; B – the effect of oxamic acid (OXA) treatment on spherogenic (BT) and adherent BT (BTadh) cell numbers; viable cell count was determined by trypan blue exclusion; * - P value is 0.0294 (one-way ANOVA,

Bonferroni`s multiple comparisons test for BTadh ctrl and OXA); error bars represent standard deviation; representative of two experiments; C - oxygen consumption rates in CSC compared with adherent BT and astrocytes; OCR in GBM CSC (BT) is significantly lower than in differentiated CSC (BT adh) and astrocytes; measurements were made for 50000 cells/well, and each data point represents an independent experiment (mean for 5 wells). The horizontal line represents the mean of 3 experiments and the error bar corresponds to SEM; ns – not significant, ***- P<0.0005 (one-way ANOVA with Bonferroni`s multiple comparisons test), * - P value is 0.0161 (two-tailed paired t-test for comparison of BT (with ctrl shRNA) and BT with Imp2 shRNA);

Supplemental Table 1. *mRNAs bound by Imp2 in GBM CSC;* List of microarray analysis of mRNA immunoprecipitated with anti-Imp2 antibody; only probesets that have rank-products false discovery rate FDR < 0.05 and fold change |M| > 2 included;

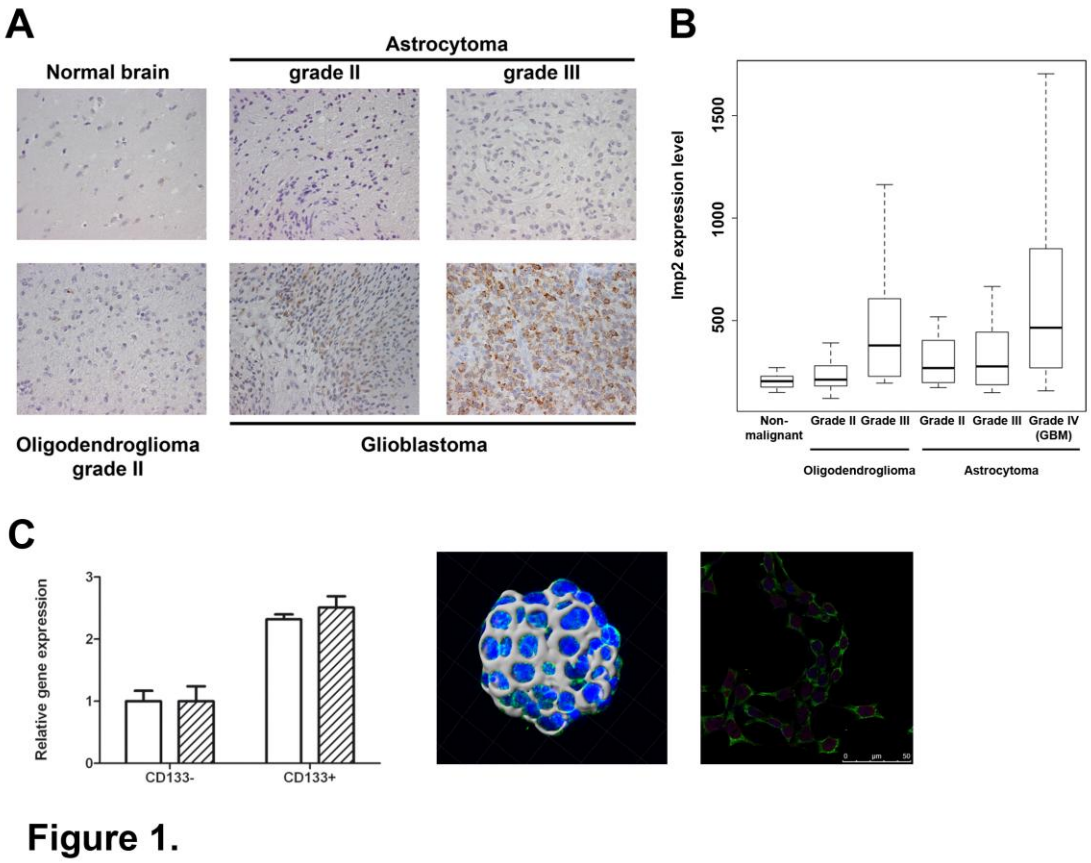

Figure 1.

A

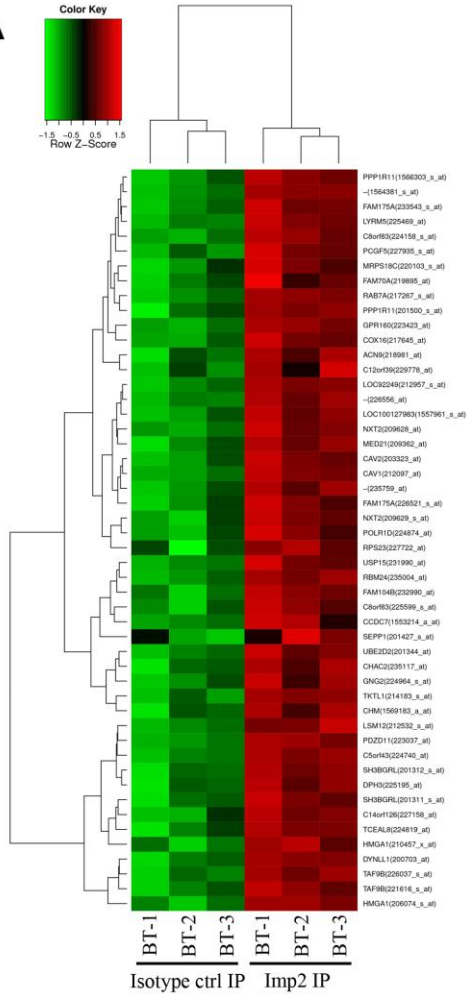

B

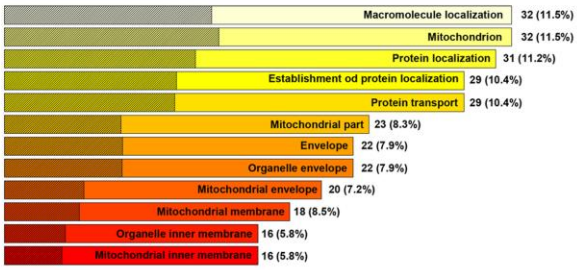

C

Identified Proteins	Accession Number	Molecular Weight	Fisher's Exact Test (P-Value)	Isotype IP	Anti-Imp2 IP
Insulin-like growth factor 2 mRNA-binding protein 2	IF2B2_HUMAN	66 kDa	95% (0.000000016)	3	36
Ubiquitin conjugation factor E4 A	UBE4A_HUMAN	123 kDa	95% (0.0000000034)	0	5
NADH dehydrogenase [ubiquinone] iron-sulfur protein 3, mitochondrial	NDUS3_HUMAN	30 kDa	95% (0.00000022)	0	22
Diaphanous homolog 2 (Drosophila), isoform CRA_c	A6NML8_HUMAN (+5)	125 kDa	95% (0.00000089)	0	20
NADH dehydrogenase [ubiquinone] iron-sulfur protein 7, mitochondrial	NDUS7_HUMAN (+1)	24 kDa	95% (0.0019)	0	9
NADH dehydrogenase [ubiquinone] 1 alpha subcomplex assembly factor 3	NDUF3_HUMAN	20 kDa	95% (0.0038)	0	8
SCY1-like protein 2	SCYL2_HUMAN	104 kDa	95% (0.0076)	0	7
Myocyte-specific enhancer factor 2D	MEF2D_HUMAN (+1)	56 kDa	95% (0.015)	0	6
Putative helicase MOV-10	MOV10_HUMAN (+1)	114 kDa	95% (0.031)	0	5
Oxysterol-binding protein-related protein 11	OSB11_HUMAN	84 kDa	95% (0.031)	0	5
NADH dehydrogenase (Ubiquinone) 1 alpha subcomplex, 5, 13kDa, isoform CRA_b	B2RD98_HUMAN (+1)	13 kDa	95% (0.031)	0	5

D

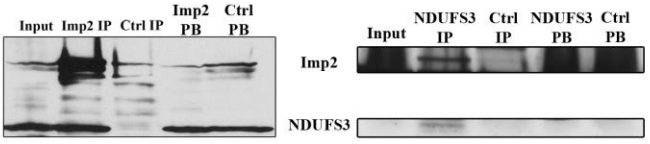

Figure 2.

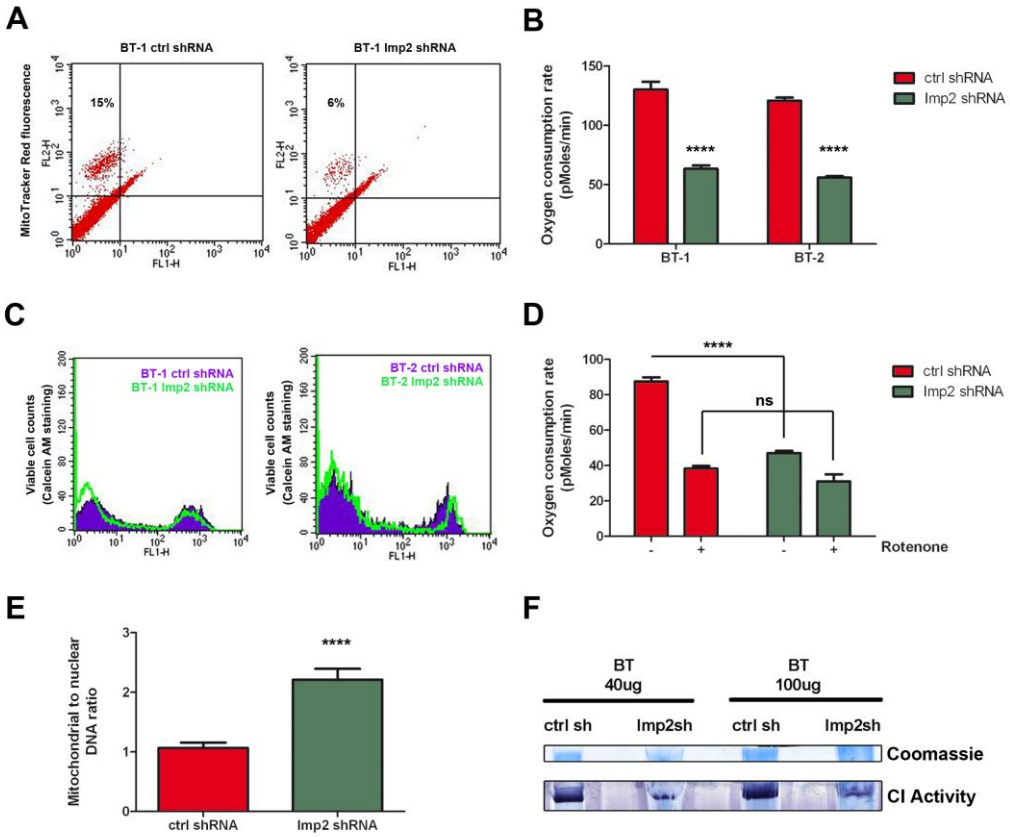

Figure 4.

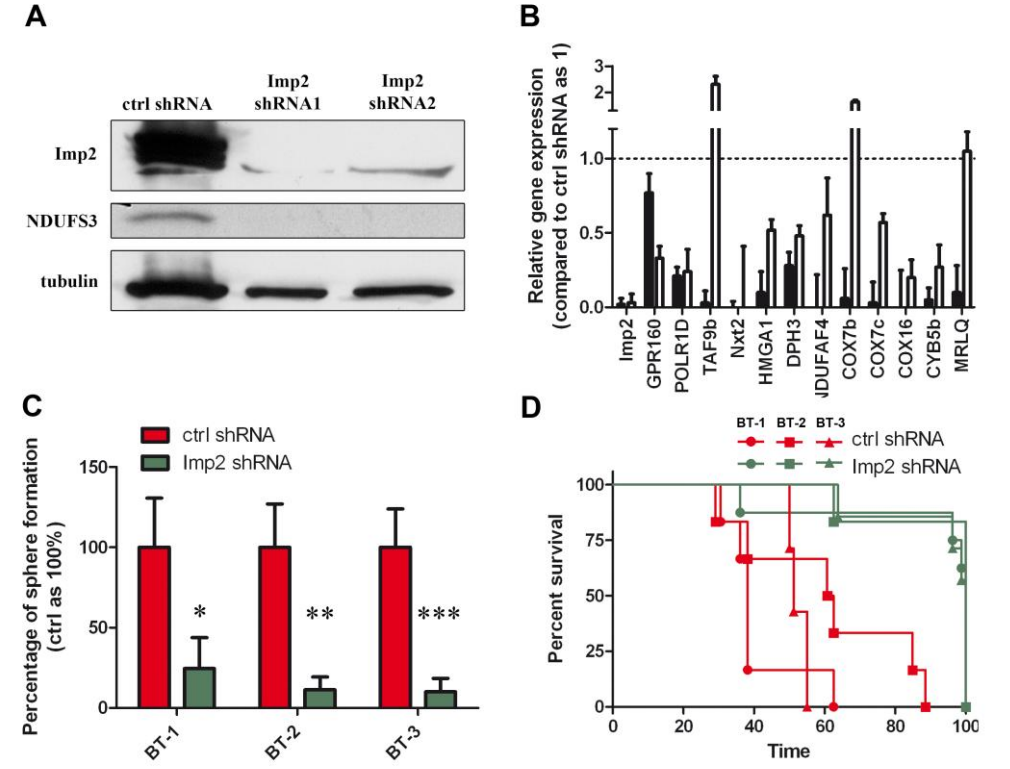

Figure 3.

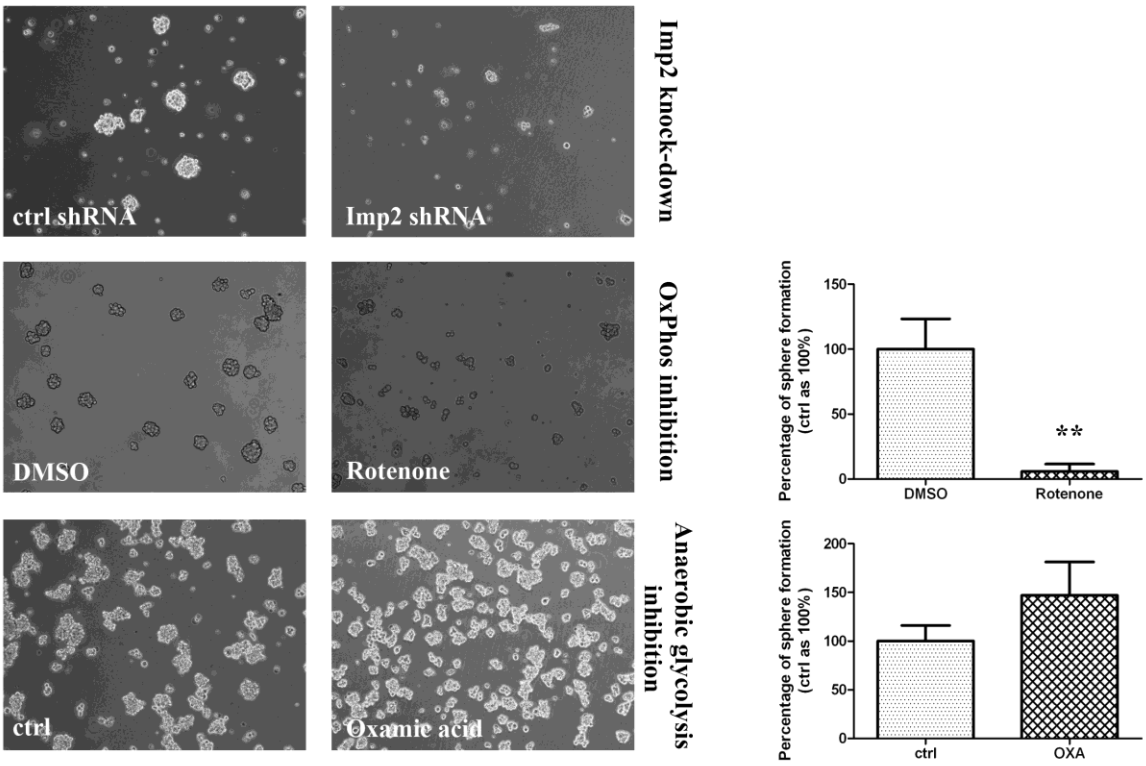

Figure 5.

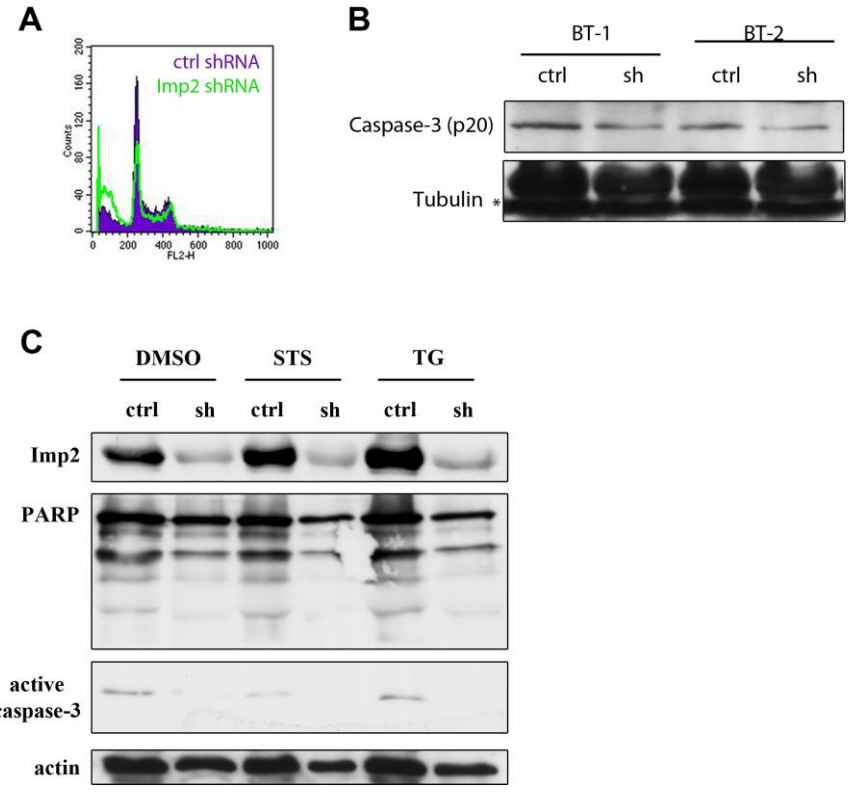

Supplemental Figure 1.

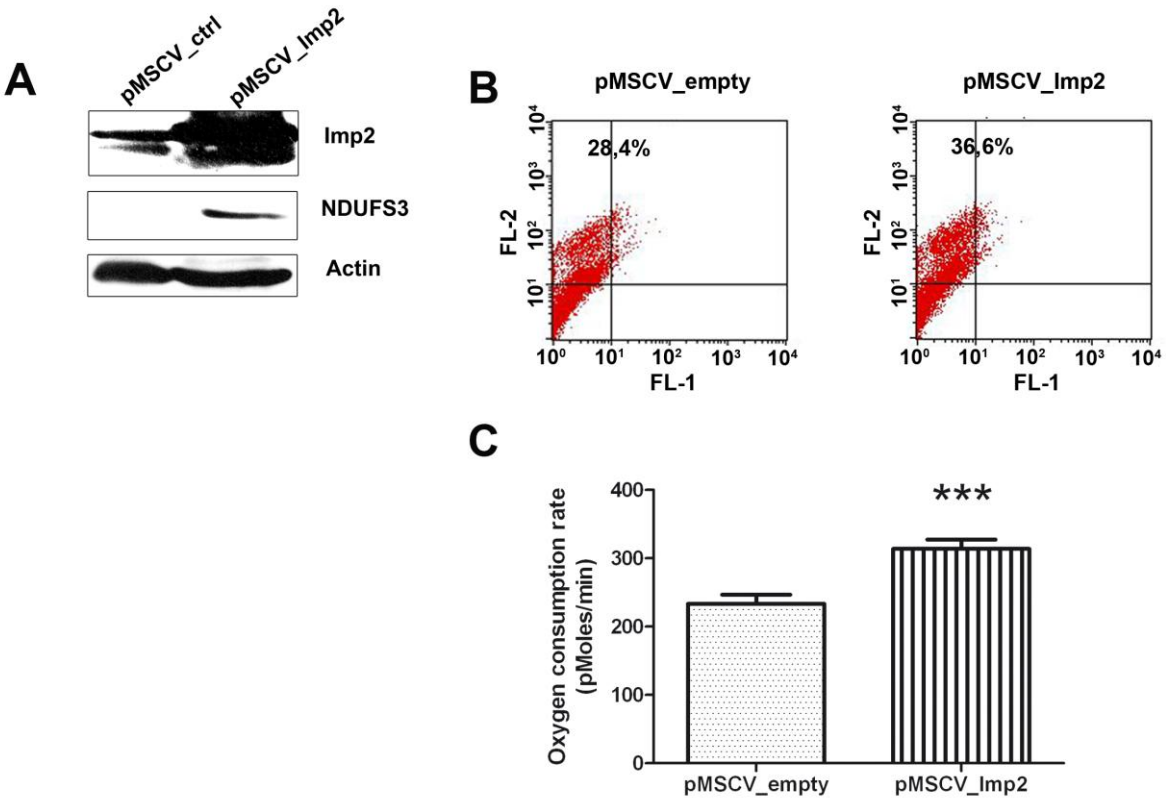

Supplemental Figure 2.

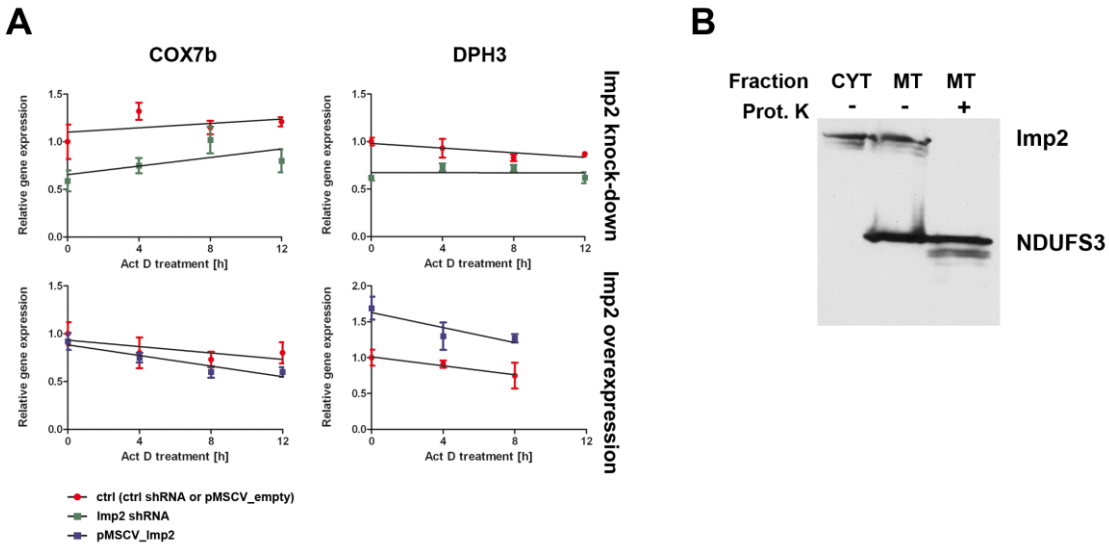

Supplemental Figure 3.

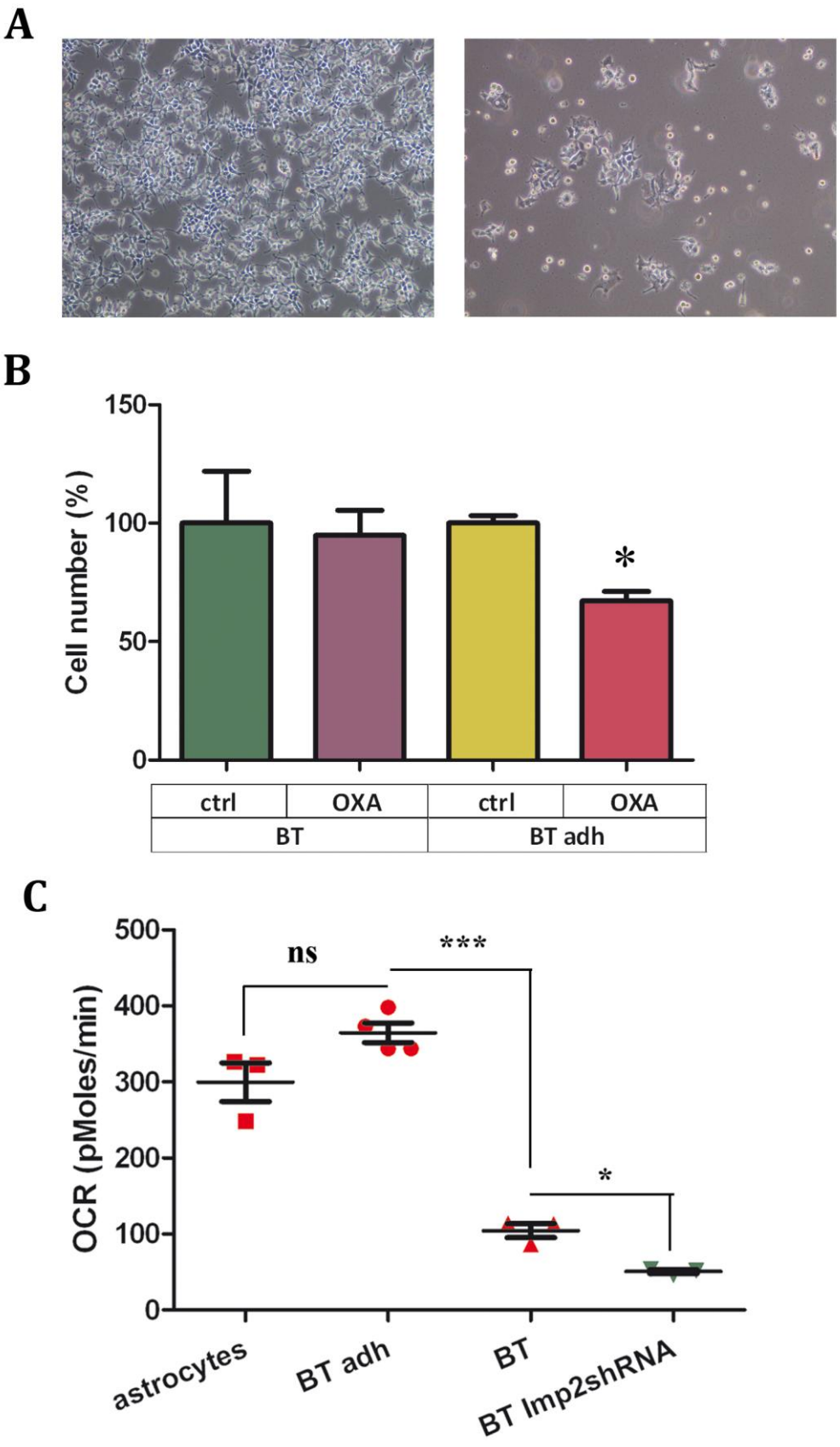

Supplemental Figure 4.

probeset	gene_id	gene_symbol	gene_name	fold change	pfp
223423_at	26996	GPR160	G protein-coupled receptor 160	4.0806	0
217645_at	51241	COX16	COX16 cytochrome c oxidase assembly homolog (S. cerevisiae)	3.8252	0
206074_s_at	3159	HMGA1	high mobility group AT-hook 1	3.8807	0
224874_at	51082	POLR1D	polymerase (RNA) I polypeptide D, 16kDa	3.5445	0
210457_x_at	3159	HMGA1	high mobility group AT-hook 1	3.5982	0
224964_s_at	54331	GNG2	guanine nucleotide binding protein (G protein), gamma 2	3.4995	0
209628_at	55916	NXT2	nuclear transport factor 2-like export factor 2	3.4149	0
209362_at	9412	MED21	mediator complex subunit 21	3.4134	0
227722_at	6228	RPS23	ribosomal protein S23	3.4569	0
1553214_a_at	221016	CCDC7	coiled-coil domain containing 7	3.2871	0
1569183_a_at	1121	CHM	choroideremia (Rab escort protein 1)	3.3016	0
224819_at	90843	TCEAL8	transcription elongation factor A (SII)-like 8	3.2376	0
233543_s_at	84142	FAM175A	family with sequence similarity 175, member A	3.2081	0
201312_s_at	6451	SH3BGRL	SH3 domain binding glutamic acid-rich protein like	3.2239	0
209629_s_at	55916	NXT2	nuclear transport factor 2-like export factor 2	3.1827	0
224740_at	643155	C5orf43	chromosome 5 open reading frame 43	3.0879	6.00E-04
1566303_s_at	6992	PPP1R11	protein phosphatase 1, regulatory (inhibitor) subunit 11	3.0895	6.00E-04
1564381_s_at	-	-	-	3.0526	6.00E-04
225195_at	285381	DPH3	DPH3, KTI11 homolog (S. cerevisiae)	2.983	5.00E-04
232990_at	90736	FAM104B	family with sequence similarity 104, member B	2.9878	5.00E-04
220103_s_at	51023	MRPS18C	mitochondrial ribosomal protein S18C	2.9853	5.00E-04
201500_s_at	6992	PPP1R11	protein phosphatase 1, regulatory (inhibitor) subunit 11	2.9472	5.00E-04
214183_s_at	8277	TKTL1	transketolase-like 1	2.9712	4.00E-04
227158_at	112487	C14orf126	chromosome 14 open reading frame 126	2.972	4.00E-04
225599_s_at	286144	C8orf83	chromosome 8 open reading frame 83	2.9058	4.00E-04
225469_at	144363	LYRM5	LYR motif containing 5	2.9068	4.00E-04

235117_at	494143	CHAC2	ChaC, cation transport regulator homolog 2 (E. coli)	2.8999	4.00E-04
212097_at	857	CAV1	caveolin 1, caveolae protein, 22kDa	2.8756	4.00E-04
226556_at	-	-	-	2.8904	3.00E-04
231990_at	9958	USP15	ubiquitin specific peptidase 15	2.9044	3.00E-04
235004_at	221662	RBM24	RNA binding motif protein 24	2.8747	3.00E-04
227935_s_at	84333	PCGF5	polycomb group ring finger 5	2.8294	3.00E-04
1557961_s_at	1E+08	LOC100127983	hypothetical protein LOC100127983	2.855	3.00E-04
203323_at	858	CAV2	caveolin 2	2.8407	3.00E-04
212532_s_at	124801	LSM12	LSM12 homolog (S. cerevisiae)	2.8577	3.00E-04
224158_s_at	286144	C8orf83	chromosome 8 open reading frame 83	2.8062	3.00E-04
219895_at	55026	FAM70A	family with sequence similarity 70, member A	2.8224	3.00E-04
217267_s_at	7879	RAB7A	RAB7A, member RAS oncogene family	2.8039	3.00E-04
235759_at	-	-	-	2.7859	3.00E-04
226037_s_at	51616	TAF9B	TAF9B RNA polymerase II, TATA box binding protein (TBP)-associated factor, 31kDa	2.7717	2.00E-04
218981_at	57001	ACN9	ACN9 homolog (S. cerevisiae)	2.7566	2.00E-04
221616_s_at	51616	TAF9B	TAF9B RNA polymerase II, TATA box binding protein (TBP)-associated factor, 31kDa	2.7366	2.00E-04
201427_s_at	6414	SEPP1	selenoprotein P, plasma, 1	2.7662	2.00E-04
212957_s_at	92249	LOC92249	hypothetical LOC92249	2.7378	2.00E-04
201311_s_at	6451	SH3BGRL	SH3 domain binding glutamic acid-rich protein like	2.7182	2.00E-04
200703_at	8655	DYNLL1	dynein, light chain, LC8-type 1	2.7417	2.00E-04
223037_at	51248	PDZD11	PDZ domain containing 11	2.7212	2.00E-04
226521_s_at	84142	FAM175A	family with sequence similarity 175, member A	2.725	2.00E-04
229778_at	80763	C12orf39	chromosome 12 open reading frame 39	2.6247	2.00E-04
201344_at	7322	UBE2D2	ubiquitin-conjugating enzyme E2D 2 (UBC4/5 homolog, yeast)	2.7037	4.00E-04
231819_at	-	-	-	2.7097	4.00E-04
218316_at	26520	TIMM9	translocase of inner mitochondrial membrane 9 homolog (yeast)	2.699	4.00E-04
212440_at	11017	SNRNP27	small nuclear ribonucleoprotein 27kDa (U4/U6.U5)	2.721	4.00E-04

219926_at	64208	POPDC3	popeye domain containing 3	2.7062	4.00E-04
225976_at	91408	BTF3L4	basic transcription factor 3-like 4	2.6843	4.00E-04
1555766_a_at	54331	GNG2	guanine nucleotide binding protein (G protein), gamma 2	2.6675	5.00E-04
201310_s_at	9315	C5orf13	chromosome 5 open reading frame 13	2.6712	5.00E-04
226010_at	79085	SLC25A23	solute carrier family 25 (mitochondrial carrier; phosphate carrier), member 23	2.66	5.00E-04
227669_at	25874	BRP44	brain protein 44	2.6661	5.00E-04
1553801_a_at	112487	C14orf126	chromosome 14 open reading frame 126	2.6879	5.00E-04
225684_at	348235	SKA2	spindle and kinetochore associated complex subunit 2	2.6746	5.00E-04
225600_at	286144	C8orf83	chromosome 8 open reading frame 83	2.6703	5.00E-04
1553321_a_at	27233	SULT1C4	sulfotransferase family, cytosolic, 1C, member 4	2.6574	5.00E-04
1558586_at	7582	ZNF33B	zinc finger protein 33B	2.6631	5.00E-04
222447_at	51108	METTL9	methyltransferase like 9	2.661	5.00E-04
226775_at	56943	ENY2	enhancer of yellow 2 homolog (Drosophila)	2.6626	5.00E-04
224965_at	54331	GNG2	guanine nucleotide binding protein (G protein), gamma 2	2.6534	4.00E-04
211597_s_at	84525	HOPX	HOP homeobox	2.6151	4.00E-04
224767_at	6167	RPL37	ribosomal protein L37	2.6473	4.00E-04
219596_at	56906	THAP10	THAP domain containing 10	2.6139	4.00E-04
243444_at	-	-	-	2.6406	4.00E-04
208656_s_at	10983	CCNI	cyclin I	2.6564	6.00E-04
226776_at	56943	ENY2	enhancer of yellow 2 homolog (Drosophila)	2.6444	5.00E-04
228483_s_at	51616	TAF9B	TAF9B RNA polymerase II, TATA box binding protein (TBP)-associated factor, 31kDa	2.6139	5.00E-04
224587_at	10923	SUB1	SUB1 homolog (S. cerevisiae)	2.6355	5.00E-04
227299_at	10983	CCNI	cyclin I	2.614	5.00E-04
202678_at	2958	GTF2A2	general transcription factor IIA, 2, 12kDa	2.6234	5.00E-04
217551_at	441453	LOC441453	similar to olfactory receptor, family 7, subfamily A, member 17	2.611	5.00E-04
1570243_at	440731	-	-	2.6202	5.00E-04
1554167_a_at	51125	GOLGA7	golgi autoantigen, golgin subfamily a, 7	2.611	5.00E-04

239988_at	-	-	-	2.5906	5.00E-04
223784_at	57393	TMEM27	transmembrane protein 27	2.5672	5.00E-04
230433_at	729970	LOC729970	similar to hCG2028352	2.5634	5.00E-04
242317_at	25994	HIGD1A	HIG1 hypoxia inducible domain family, member 1A	2.5845	5.00E-04
1553133_at	203228	C9orf72	chromosome 9 open reading frame 72	2.6042	5.00E-04
201745_at	5756	TWF1	twinfilin, actin-binding protein, homolog 1 (Drosophila)	2.6102	5.00E-04
225053_at	29883	CNOT7	CCR4-NOT transcription complex, subunit 7	2.5883	5.00E-04
1555906_s_at	285343	C3orf23	chromosome 3 open reading frame 23	2.5883	5.00E-04
225603_s_at	286144	C8orf83	chromosome 8 open reading frame 83	2.6039	4.00E-04
1555905_a_at	285343	C3orf23	chromosome 3 open reading frame 23	2.581	4.00E-04
240711_at	-	-	-	2.5945	4.00E-04
225028_at	550643	LOC550643	hypothetical LOC550643	2.5738	4.00E-04
218930_s_at	54664	TMEM106B	transmembrane protein 106B	2.5928	4.00E-04
230560_at	29091	STXBP6	syntaxin binding protein 6 (amisyn)	2.5473	4.00E-04
241959_at	10393	ANAPC10	anaphase promoting complex subunit 10	2.5625	4.00E-04
226338_at	55529	TMEM55A	transmembrane protein 55A	2.5589	4.00E-04
243998_at	125113	KRT222	keratin 222	2.5454	4.00E-04
205569_at	27074	LAMP3	lysosomal-associated membrane protein 3	2.535	4.00E-04
228107_at	1E+08	LOC100127983	hypothetical protein LOC100127983	2.569	6.00E-04
222487_s_at	51065	RPS27L	ribosomal protein S27-like	2.5425	6.00E-04
202543_s_at	2764	GMFB	glia maturation factor, beta	2.5476	6.00E-04
240712_s_at	-	-	-	2.5402	6.00E-04
217988_at	57820	CCNB1IP1	cyclin B1 interacting protein 1	2.5448	6.00E-04
230174_at	127018	LYPLAL1	lysophospholipase-like 1	2.5103	6.00E-04
218946_at	27247	NFU1	NFU1 iron-sulfur cluster scaffold homolog (S. cerevisiae)	2.5267	7.00E-04
222948_s_at	51023	MRPS18C	mitochondrial ribosomal protein S18C	2.4951	7.00E-04
225580_at	54534	MRPL50	mitochondrial ribosomal protein L50	2.5483	7.00E-04

202544_at	2764	GMFB	glia maturation factor, beta	2.538	6.00E-04
241017_at	11138	TBC1D8	TBC1 domain family, member 8 (with GRAM domain)	2.4543	6.00E-04
235429_at	-	-	-	2.4963	6.00E-04
218139_s_at	55745	MUDENG	MU-2/AP1M2 domain containing, death-inducing	2.4558	6.00E-04
221726_at	6146	RPL22	ribosomal protein L22	2.5196	6.00E-04
218007_s_at	51065	RPS27L	ribosomal protein S27-like	2.5001	6.00E-04
212595_s_at	9802	DAZAP2	DAZ associated protein 2	2.5096	6.00E-04
223266_at	55437	STRADB	STE20-related kinase adaptor beta	2.5086	6.00E-04
241652_x_at	-	-	-	2.5042	6.00E-04
201691_s_at	7163	TPD52	tumor protein D52	2.4875	6.00E-04
226596_x_at	729852	tcag7.903	hypothetical protein LOC729852	2.4883	6.00E-04
225105_at	387882	C12orf75	chromosome 12 open reading frame 75	2.4994	7.00E-04
217816_s_at	57092	PCNP	PEST proteolytic signal containing nuclear protein	2.5058	8.00E-04
203324_s_at	858	CAV2	caveolin 2	2.4735	7.00E-04
229793_at	653308	ASAH2B	N-acylsphingosine amidohydrolase (non-lysosomal ceramidase) 2B	2.4755	7.00E-04
235696_at	-	-	-	2.4689	8.00E-04
229146_at	136895	C7orf31	chromosome 7 open reading frame 31	2.4216	8.00E-04
207276_at	1038	CDR1	cerebellar degeneration-related protein 1, 34kDa	2.4725	8.00E-04
240027_at	8825	LIN7A	lin-7 homolog A (C. elegans)	2.4693	8.00E-04
209139_s_at	8575	PRKRA	protein kinase, interferon-inducible double stranded RNA dependent activator	2.4234	9.00E-04
214033_at	368	ABCC6	ATP-binding cassette, sub-family C (CFTR/MRP), member 6	2.423	9.00E-04
201708_s_at	8508	NIPSNAP1	nipsnap homolog 1 (C. elegans)	2.427	9.00E-04
203303_at	6990	DYNLT3	dynein, light chain, Tctex-type 3	2.435	9.00E-04
223071_at	51124	IER3IP1	immediate early response 3 interacting protein 1	2.4648	9.00E-04
239252_at	-	-	-	2.3586	0.001
206238_s_at	10138	YAF2	YY1 associated factor 2	2.423	0.0011
200706_s_at	9516	LITAF	lipopolysaccharide-induced TNF factor	2.4156	0.001

221727_at	10923	SUB1	SUB1 homolog (S. cerevisiae)	2.438	0.001
224584_at	29058	C20orf30	chromosome 20 open reading frame 30	2.4271	0.001
235354_s_at	51319	RSRC1	arginine/serine-rich coiled-coil 1	2.4334	0.001
226633_at	51762	RAB8B	RAB8B, member RAS oncogene family	2.3594	0.001
242905_at	56902	PNO1	partner of NOB1 homolog (S. cerevisiae)	2.4279	0.001
231640_at	-	-	-	2.4199	0.001
1559005_s_at	54875	CNTLN	centlein, centrosomal protein	2.4289	0.0011
1568951_at	54816	ZNF280D	zinc finger protein 280D	2.3804	0.0011
214658_at	51014	TMED7	transmembrane emp24 protein transport domain containing 7	2.3983	0.0011
222750_s_at	79644	SRD5A3	steroid 5 alpha-reductase 3	2.4004	0.0011
223667_at	51661	FKBP7	FK506 binding protein 7	2.4291	0.0011
203622_s_at	56902	PNO1	partner of NOB1 homolog (S. cerevisiae)	2.3911	0.0012
204017_at	11015	KDELR3	KDEL (Lys-Asp-Glu-Leu) endoplasmic reticulum protein retention receptor 3	2.3695	0.0012
225413_at	84833	USMG5	up-regulated during skeletal muscle growth 5 homolog (mouse)	2.3902	0.0011
223087_at	55862	ECHDC1	enoyl Coenzyme A hydratase domain containing 1	2.3919	0.0013
225029_at	550643	LOC550643	hypothetical LOC550643	2.3666	0.0014
225399_at	116461	TSEN15	tRNA splicing endonuclease 15 homolog (S. cerevisiae)	2.3487	0.0014
204795_at	80742	PRR3	proline rich 3	2.3373	0.0014
203007_x_at	10434	LYPLA1	lysophospholipase I	2.3438	0.0014
225926_at	10490	VTI1B	vesicle transport through interaction with t-SNAREs homolog 1B (yeast)	2.3095	0.0017
201002_s_at	7335	UBE2V1	ubiquitin-conjugating enzyme E2 variant 1	2.3941	0.0017
243887_at	-	-	-	2.3579	0.0017
225692_at	23261	CAMTA1	calmodulin binding transcription activator 1	2.3984	0.0018
221620_s_at	79135	APOO	apolipoprotein O	2.3628	0.0018
209363_s_at	9412	MED21	mediator complex subunit 21	2.3665	0.0018
230570_at	-	-	-	2.3365	0.0018
209714_s_at	1033	CDKN3	cyclin-dependent kinase inhibitor 3	2.3616	0.0018

219318_x_at	51003	MED31	mediator complex subunit 31	2.3694	0.0018
229174_at	285237	C3orf38	chromosome 3 open reading frame 38	2.3253	0.0018
218545_at	55297	CCDC91	coiled-coil domain containing 91	2.3509	0.0018
231538_at	64776	C11orf1	chromosome 11 open reading frame 1	2.3463	0.0018
218404_at	29887	SNX10	sorting nexin 10	2.3426	0.0017
229744_at	6744	SSFA2	sperm specific antigen 2	2.2639	0.0018
222834_s_at	55970	GNG12	guanine nucleotide binding protein (G protein), gamma 12	2.3355	0.0018
212055_at	25941	C18orf10	chromosome 18 open reading frame 10	2.3564	0.0019
236473_at	57545	CC2D2A	coiled-coil and C2 domain containing 2A	2.1944	0.0019
222734_at	10352	WARS2	tryptophanyl tRNA synthetase 2, mitochondrial	2.3083	0.0019
201634_s_at	80777	CYB5B	cytochrome b5 type B (outer mitochondrial membrane)	2.3037	0.0019
201689_s_at	7163	TPD52	tumor protein D52	2.3188	0.002
231764_at	54108	CHRAC1	chromatin accessibility complex 1	2.3608	0.002
226276_at	153339	TMEM167A	transmembrane protein 167A	2.3452	0.0019
225400_at	116461	TSEN15	tRNA splicing endonuclease 15 homolog (S. cerevisiae)	2.3403	0.002
222846_at	51762	RAB8B	RAB8B, member RAS oncogene family	2.2115	0.0021
207265_s_at	11015	KDELR3	KDEL (Lys-Asp-Glu-Leu) endoplasmic reticulum protein retention receptor 3	2.3432	0.0022
214007_s_at	5756	TWF1	twinfilin, actin-binding protein, homolog 1 (Drosophila)	2.3483	0.0022
200864_s_at	8766	RAB11A	RAB11A, member RAS oncogene family	2.2929	0.0022
1555758_a_at	1033	CDKN3	cyclin-dependent kinase inhibitor 3	2.3171	0.0023
230413_s_at	-	-	-	2.3422	0.0023
202142_at	10920	COPS8	COP9 constitutive photomorphogenic homolog subunit 8 (Arabidopsis)	2.3226	0.0022
212529_at	124801	LSM12	LSM12 homolog (S. cerevisiae)	2.3342	0.0022
221617_at	51616	TAF9B	TAF9B RNA polymerase II, TATA box binding protein (TBP)-associated factor, 31kDa	2.3307	0.0022
202919_at	25843	MOBKL3	MOB1, Mps One Binder kinase activator-like 3 (yeast)	2.3235	0.0023
230122_at	8028	MLLT10	myeloid/lymphoid or mixed-lineage leukemia (trithorax homolog, Drosophila); translocated to, 10	2.2765	0.0022
201309_x_at	9315	C5orf13	chromosome 5 open reading frame 13	2.3372	0.0022

200902_at	9403	sept.15	15 kDa selenoprotein	2.3333	0.0022
224650_at	114569	MAL2	mal, T-cell differentiation protein 2	2.2686	0.0022
238675_x_at	91408	BTF3L4	basic transcription factor 3-like 4	2.3014	0.0022
209274_s_at	81689	ISCA1	iron-sulfur cluster assembly 1 homolog (S. cerevisiae)	2.2945	0.0022
225940_at	317649	EIF4E3	eukaryotic translation initiation factor 4E family member 3	2.309	0.0022
222785_x_at	64776	C11orf1	chromosome 11 open reading frame 1	2.3185	0.0022
218800_at	79644	SRD5A3	steroid 5 alpha-reductase 3	2.2531	0.0022
226190_at	-	-	-	2.3259	0.0022
210802_s_at	27292	DIMT1L	DIM1 dimethyladenosine transferase 1-like (S. cerevisiae)	2.3206	0.0022
200704_at	9516	LITAF	lipopolysaccharide-induced TNF factor	2.2715	0.0022
235819_at	-	-	-	2.3028	0.0023
217971_at	8649	MAPKSP1	MAPK scaffold protein 1	2.2929	0.0023
214762_at	534	ATP6V1G2	ATPase, H+ transporting, lysosomal 13kDa, V1 subunit G2	2.2451	0.0022
200941_at	3281	HSBP1	heat shock factor binding protein 1	2.2808	0.0022
224751_at	647087	PL-5283	PL-5283 protein	2.2971	0.0023
227559_at	29078	NDUFAF4	NADH dehydrogenase (ubiquinone) 1 alpha subcomplex, assembly factor 4	2.2543	0.0024
214823_at	7754	ZNF204	zinc finger protein 204 pseudogene	2.3009	0.0024
230376_at	2958	GTF2A2	general transcription factor IIA, 2, 12kDa	2.2238	0.0025
227711_at	121355	GTSF1	gametocyte specific factor 1	2.3011	0.0026
203858_s_at	1352	COX10	COX10 homolog, cytochrome c oxidase assembly protein, heme A: farnesyltransferase (yeast)	2.259	0.0026
218668_s_at	57826	RAP2C	RAP2C, member of RAS oncogene family	2.2599	0.0027
238803_at	143279	HECTD2	HECT domain containing 2	2.2611	0.0027
1552344_s_at	29883	CNOT7	CCR4-NOT transcription complex, subunit 7	2.2225	0.0027
203799_at	9936	CD302	CD302 molecule	2.2926	0.0026
224690_at	116151	C20orf108	chromosome 20 open reading frame 108	2.2278	0.0026
225693_s_at	23261	CAMTA1	calmodulin binding transcription activator 1	2.2885	0.0027
222679_s_at	54165	DCUN1D1	DCN1, defective in cullin neddylation 1, domain containing 1 (S. cerevisiae)	2.1801	0.0027

218379_at	10179	RBM7	RNA binding motif protein 7	2.2759	0.0027
211071_s_at	10962	MLLT11	myeloid/lymphoid or mixed-lineage leukemia (trithorax homolog, Drosophila); translocated to, 11	2.2826	0.0027
1554868_s_at	57092	PCNP	PEST proteolytic signal containing nuclear protein	2.2712	0.0027
222466_s_at	28977	MRPL42	mitochondrial ribosomal protein L42	2.2833	0.0027
212837_at	23172	FAM175B	family with sequence similarity 175, member B	2.2444	0.0027
214676_x_at	4584	MUC3A	mucin 3A, cell surface associated	2.2061	0.0027
210125_s_at	8815	BANF1	barrier to autointegration factor 1	2.2648	0.0027
217989_at	51170	HSD17B11	hydroxysteroid (17-beta) dehydrogenase 11	2.2774	0.0027
208025_s_at	8091	HMGA2	high mobility group AT-hook 2	2.2816	0.0027
217827_s_at	51324	SPG21	spastic paraplegia 21 (autosomal recessive, Mast syndrome)	2.2627	0.0027
202345_s_at	2171	FABP5	fatty acid binding protein 5 (psoriasis-associated)	2.2797	0.0027
243237_at	-	-	-	2.2026	0.0027
218174_s_at	80195	C10orf57	chromosome 10 open reading frame 57	2.1884	0.0027
225581_s_at	54534	MRPL50	mitochondrial ribosomal protein L50	2.2755	0.0027
206928_at	7678	ZNF124	zinc finger protein 124	2.2214	0.0027
236721_at	8846	ALKBH1	alkB, alkylation repair homolog 1 (E. coli)	2.2283	0.0028
218583_s_at	54165	DCUN1D1	DCN1, defective in cullin neddylation 1, domain containing 1 (S. cerevisiae)	2.2732	0.0028
231530_s_at	64776	C11orf1	chromosome 11 open reading frame 1	2.2491	0.0028
205184_at	2786	GNG4	guanine nucleotide binding protein (G protein), gamma 4	2.2518	0.0028
211758_x_at	10190	TXNDC9	thioredoxin domain containing 9	2.2626	0.0028
238465_at	133383	C5orf35	chromosome 5 open reading frame 35	2.2334	0.0028
222637_at	51397	COMMD10	COMM domain containing 10	2.2746	0.0028
218467_at	56984	PSMG2	proteasome (prosome, macropain) assembly chaperone 2	2.2648	0.0028
218784_s_at	55776	C6orf64	chromosome 6 open reading frame 64	2.167	0.0028
220198_s_at	56648	EIF5A2	eukaryotic translation initiation factor 5A2	2.2224	0.0028
219288_at	57415	C3orf14	chromosome 3 open reading frame 14	2.2643	0.0028
209404_s_at	51014	TMED7	transmembrane emp24 protein transport domain containing 7	2.2409	0.0029

230921_s_at	-	-	-	2.2646	0.0029
219210_s_at	51762	RAB8B	RAB8B, member RAS oncogene family	2.2209	0.0029
208819_at	4218	RAB8A	RAB8A, member RAS oncogene family	2.235	0.0029
228142_at	29796	UCRC	ubiquinol-cytochrome c reductase complex (7.2 kD)	2.1925	0.0029
218899_s_at	79870	BAALC	brain and acute leukemia, cytoplasmic	2.0691	0.0029
229145_at	119504	C10orf104	chromosome 10 open reading frame 104	2.1616	0.0029
212371_at	51029	PPPDE1	PPPDE peptidase domain containing 1	2.1792	0.0029
200794_x_at	9802	DAZAP2	DAZ associated protein 2	2.2288	0.003
225228_at	128338	DRAM2	DNA-damage regulated autophagy modulator 2	2.1891	0.003
218212_s_at	4338	MOCS2	molybdenum cofactor synthesis 2	2.2206	0.003
1556736_at	1E+08	LOC100129858	hypothetical protein LOC100129858	2.1791	0.003
226751_at	25927	CNRIP1	cannabinoid receptor interacting protein 1	2.2125	0.003
217868_s_at	51108	METTL9	methyltransferase like 9	2.1829	0.0031
235155_at	56898	BDH2	3-hydroxybutyrate dehydrogenase, type 2	2.139	0.0031
202110_at	1349	COX7B	cytochrome c oxidase subunit VIIb	2.2236	0.0032
203065_s_at	857	CAV1	caveolin 1, caveolae protein, 22kDa	2.2225	0.0032
1555765_a_at	2786	GNG4	guanine nucleotide binding protein (G protein), gamma 4	2.2159	0.0032
227534_at	195827	C9orf21	chromosome 9 open reading frame 21	2.1725	0.0032
224641_at	84248	FYTTD1	forty-two-three domain containing 1	2.2279	0.0031
213263_s_at	5094	PCBP2	poly(rC) binding protein 2	2.2211	0.0032
208745_at	10632	ATP5L	ATP synthase, H+ transporting, mitochondrial F0 complex, subunit G	2.1882	0.0033
226220_at	51108	METTL9	methyltransferase like 9	2.1683	0.0034
231102_at	54677	CROT	carnitine O-octanoyltransferase	2.1467	0.0034
212751_at	7334	UBE2N	ubiquitin-conjugating enzyme E2N (UBC13 homolog, yeast)	2.1868	0.0034
208770_s_at	1979	EIF4EBP2	eukaryotic translation initiation factor 4E binding protein 2	2.2	0.0034
235362_at	729970	LOC729970	similar to hCG2028352	2.1489	0.0034
209771_x_at	1E+08	CD24	CD24 molecule	2.2053	0.0033

238574_at	92014	MCART1	mitochondrial carrier triple repeat 1	2.1481	0.0033
224971_at	51263	MRPL30	mitochondrial ribosomal protein L30	2.2123	0.0034
212281_s_at	27346	TMEM97	transmembrane protein 97	2.1893	0.0033
232752_at	-	-	-	2.1636	0.0035
210186_s_at	2280	FKBP1A	FK506 binding protein 1A, 12kDa	2.1893	0.0035
224364_s_at	53938	PPIL3	peptidylprolyl isomerase (cyclophilin)-like 3	2.2062	0.0035
201022_s_at	11034	DSTN	destrin (actin depolymerizing factor)	2.1967	0.0034
1552370_at	132321	C4orf33	chromosome 4 open reading frame 33	2.2061	0.0034
204031_s_at	5094	PCBP2	poly(rC) binding protein 2	2.2006	0.0035
228391_at	285440	CYP4V2	cytochrome P450, family 4, subfamily V, polypeptide 2	2.1564	0.0034
201690_s_at	7163	TPD52	tumor protein D52	2.1907	0.0035
223551_at	5570	PKIB	protein kinase (cAMP-dependent, catalytic) inhibitor beta	2.1804	0.0035
200823_x_at	6159	RPL29	ribosomal protein L29	2.194	0.0035
224693_at	116151	C20orf108	chromosome 20 open reading frame 108	2.1716	0.0035
202165_at	5504	PPP1R2	protein phosphatase 1, regulatory (inhibitor) subunit 2	2.1764	0.0036
203008_x_at	10190	TXNDC9	thioredoxin domain containing 9	2.1776	0.0035
201380_at	10491	CRTAP	cartilage associated protein	2.1455	0.0035
212294_at	55970	GNG12	guanine nucleotide binding protein (G protein), gamma 12	2.187	0.0035
235296_at	56648	EIF5A2	eukaryotic translation initiation factor 5A2	2.1455	0.0036
214812_s_at	55233	MOBKL1B	MOB1, Mps One Binder kinase activator-like 1B (yeast)	2.1746	0.0036
220199_s_at	64853	AIDA	axin interactor, dorsalization associated	2.1624	0.0036
231130_at	51661	FKBP7	FK506 binding protein 7	2.1859	0.0036
209130_at	8773	SNAP23	synaptosomal-associated protein, 23kDa	2.1708	0.0036
206440_at	8825	LIN7A	lin-7 homolog A (C. elegans)	2.1799	0.0035
238164_at	9712	USP6NL	USP6 N-terminal like	2.1157	0.0035
208762_at	7341	SUMO1	SMT3 suppressor of mif two 3 homolog 1 (S. cerevisiae)	2.171	0.0035
1558819_at	1E+08	-	-	2.0422	0.0035

230787_at	-	-	-	2.125	0.0035
209806_at	85236	HIST1H2BK	histone cluster 1, H2bk	2.1848	0.0036
201297_s_at	55233	MOBKL1B	MOB1, Mps One Binder kinase activator-like 1B (yeast)	2.1879	0.0035
1561894_at	653739	LOC653739	hypothetical protein LOC653739	2.1072	0.0036
225125_at	93380	MMGT1	membrane magnesium transporter 1	2.1442	0.0036
224436_s_at	25934	NIPSNAP3A	nipsnap homolog 3A (C. elegans)	2.1787	0.0037
216379_x_at	1E+08	CD24	CD24 molecule	2.1797	0.0038
204675_at	6715	SRD5A1	steroid-5-alpha-reductase, alpha polypeptide 1 (3-oxo-5 alpha-steroid delta 4-dehydrogenase alpha 1)	2.0482	0.0038
217783_s_at	51646	YPEL5	yippee-like 5 (Drosophila)	2.1675	0.0038
201649_at	9246	UBE2L6	ubiquitin-conjugating enzyme E2L 6	2.1236	0.0038
222531_s_at	55745	MUDENG	MU-2/AP1M2 domain containing, death-inducing	2.1275	0.0038
238126_at	-	-	-	2.0119	0.0038
224752_at	647087	PL-5283	PL-5283 protein	2.149	0.004
202732_at	11142	PKIG	protein kinase (cAMP-dependent, catalytic) inhibitor gamma	2.0765	0.004
201120_s_at	10857	PGRMC1	progesterone receptor membrane component 1	2.0931	0.004
242328_at	115827	RAB3C	RAB3C, member RAS oncogene family	2.0892	0.0039
213061_s_at	123803	NTAN1	N-terminal asparagine amidase	2.126	0.0039
201435_s_at	1977	EIF4E	eukaryotic translation initiation factor 4E	2.1593	0.0039
211727_s_at	1353	COX11	COX11 homolog, cytochrome c oxidase assembly protein (yeast)	2.1018	0.0039
216241_s_at	6917	TCEA1	transcription elongation factor A (SII), 1	2.1297	0.004
227295_at	121457	IKIP	IKK interacting protein	2.1537	0.004
238461_at	317649	EIF4E3	eukaryotic translation initiation factor 4E family member 3	2.1261	0.0041
202903_at	23658	LSM5	LSM5 homolog, U6 small nuclear RNA associated (S. cerevisiae)	2.0956	0.004
207437_at	4857	NOVA1	neuro-oncological ventral antigen 1	2.1286	0.0041
214008_at	5756	TWF1	twinfilin, actin-binding protein, homolog 1 (Drosophila)	2.1541	0.004
202141_s_at	10920	COPS8	COP9 constitutive photomorphogenic homolog subunit 8 (Arabidopsis)	2.1228	0.004
205741_s_at	1837	DTNA	dystrobrevin, alpha	2.0805	0.0041

201001_s_at	7335	UBE2V1	ubiquitin-conjugating enzyme E2 variant 1	2.1381	0.0041
201302_at	307	ANXA4	annexin A4	2.0861	0.0041
208769_at	1979	EIF4EBP2	eukaryotic translation initiation factor 4E binding protein 2	2.0739	0.0041
218250_s_at	29883	CNOT7	CCR4-NOT transcription complex, subunit 7	2.0942	0.0043
230655_at	-	-	-	2.1301	0.0043
221618_s_at	51616	TAF9B	TAF9B RNA polymerase II, TATA box binding protein (TBP)-associated factor, 31kDa	2.0533	0.0046
212449_s_at	10434	LYPLA1	lysophospholipase I	2.1111	0.0047
224731_at	3146	HMGB1	high-mobility group box 1	2.1443	0.0049
212590_at	22800	RRAS2	related RAS viral (r-ras) oncogene homolog 2	2.107	0.0048
217773_s_at	4697	NDUFA4	NADH dehydrogenase (ubiquinone) 1 alpha subcomplex, 4, 9kDa	2.1214	0.0049
244114_x_at	-	-	-	2.1216	0.0049
217819_at	51125	GOLGA7	golgi autoantigen, golgin subfamily a, 7	2.0837	0.0049
230264_s_at	8905	AP1S2	adaptor-related protein complex 1, sigma 2 subunit	2.0904	0.0051
226529_at	54664	TMEM106B	transmembrane protein 106B	2.0986	0.0051
229746_x_at	-	-	-	2.1196	0.0052
208655_at	-	-	-	2.0777	0.0051
227165_at	221150	SKA3	spindle and kinetochore associated complex subunit 3	2.1129	0.0051
1555501_s_at	51319	RSRC1	arginine/serine-rich coiled-coil 1	2.1163	0.0053
222437_s_at	51652	VPS24	vacuolar protein sorting 24 homolog (S. cerevisiae)	2.0825	0.0054
241443_at	-	-	-	2.066	0.0054
202334_s_at	7320	UBE2B	ubiquitin-conjugating enzyme E2B (RAD6 homolog)	2.0593	0.0054
212833_at	91137	SLC25A46	solute carrier family 25, member 46	2.0946	0.0055
227932_at	10425	ARIH2	ariadne homolog 2 (Drosophila)	2.0662	0.0055
226745_at	285440	CYP4V2	cytochrome P450, family 4, subfamily V, polypeptide 2	2.0795	0.0056
213846_at	1350	COX7C	cytochrome c oxidase subunit VIIc	2.0832	0.0055
202166_s_at	5504	PPP1R2	protein phosphatase 1, regulatory (inhibitor) subunit 2	2.0291	0.0057
225941_at	317649	EIF4E3	eukaryotic translation initiation factor 4E family member 3	2.0803	0.0057

203466_at	4358	MPV17	MpV17 mitochondrial inner membrane protein	2.0746	0.0057
226278_at	258010	SVIP	small VCP/p97-interacting protein	2.0334	0.0058
214022_s_at	8519	IFITM1	interferon induced transmembrane protein 1 (9-27)	2.1031	0.0058
204612_at	5569	PKIA	protein kinase (cAMP-dependent, catalytic) inhibitor alpha	2.0835	0.0058
205621_at	8846	ALKBH1	alkB, alkylation repair homolog 1 (E. coli)	2.0679	0.0059
206113_s_at	5868	RAB5A	RAB5A, member RAS oncogene family	2.0838	0.006
226686_at	493856	CISD2	CDGSH iron sulfur domain 2	2.0634	0.0059
203207_s_at	9650	MTFR1	mitochondrial fission regulator 1	2.0536	0.006
200922_at	10945	KDELR1	KDEL (Lys-Asp-Glu-Leu) endoplasmic reticulum protein retention receptor 1	2.0612	0.0061
219875_s_at	51029	PPPDE1	PPPDE peptidase domain containing 1	2.0127	0.0062
224664_at	119504	C10orf104	chromosome 10 open reading frame 104	2.0505	0.0062
218643_s_at	9419	CRIPT	cysteine-rich PDZ-binding protein	2.0697	0.0062
209089_at	5868	RAB5A	RAB5A, member RAS oncogene family	2.0811	0.0062
225036_at	6461	SHB	Src homology 2 domain containing adaptor protein B	2.0829	0.0062
214119_s_at	2280	FKBP1A	FK506 binding protein 1A, 12kDa	2.064	0.0062
1557411_s_at	203427	SLC25A43	solute carrier family 25, member 43	2.0656	0.0062
219029_at	64417	C5orf28	chromosome 5 open reading frame 28	2.0366	0.0064
1556236_at	-	-	-	2.0739	0.0064
200067_x_at	8724	SNX3	sorting nexin 3	2.0621	0.0064
225939_at	317649	EIF4E3	eukaryotic translation initiation factor 4E family member 3	2.0223	0.0065
218420_s_at	80209	C13orf23	chromosome 13 open reading frame 23	2.0387	0.0064
238599_at	134728	IRAK1BP1	interleukin-1 receptor-associated kinase 1 binding protein 1	2.0212	0.0064
201399_s_at	23471	TRAM1	translocation associated membrane protein 1	2.0164	0.0064
236204_at	-	-	-	2.0542	0.0064
217837_s_at	51652	VPS24	vacuolar protein sorting 24 homolog (S. cerevisiae)	2.0437	0.0064
235010_at	729013	LOC729013	hypothetical protein LOC729013	2.0267	0.0064
244523_at	23531	MMD	monocyte to macrophage differentiation-associated	2.0478	0.0065

209065_at	7381	UQCRB	ubiquinol-cytochrome c reductase binding protein	2.0289	0.0065
218010_x_at	79144	PPDPF	pancreatic progenitor cell differentiation and proliferation factor homolog (zebrafish)	2.0758	0.0064
218163_at	28985	MCTS1	malignant T cell amplified sequence 1	2.0614	0.0065
201980_s_at	6251	RSU1	Ras suppressor protein 1	2.0709	0.0065
203561_at	2212	FCGR2A	Fc fragment of IgG, low affinity IIa, receptor (CD32)	2.0503	0.0066
213930_at	-	-	-	2.0026	0.0066
226159_at	285636	C5orf51	chromosome 5 open reading frame 51	2.0297	0.0065
231401_s_at	-	-	-	2.0323	0.0066
224577_at	57222	ERGIC1	endoplasmic reticulum-golgi intermediate compartment (ERGIC) 1	2.0135	0.0067
204420_at	8061	FOSL1	FOS-like antigen 1	2.0428	0.0068
200986_at	710	SERPING1	serpin peptidase inhibitor, clade G (C1 inhibitor), member 1	2.0548	0.0068
203897_at	57149	LYRM1	LYR motif containing 1	2.0101	0.0069
266_s_at	1E+08	CD24	CD24 molecule	2.0353	0.0072
206272_at	5867	RAB4A	RAB4A, member RAS oncogene family	2.0011	0.0075
226831_at	91137	SLC25A46	solute carrier family 25, member 46	2.0016	0.0076
235470_at	-	-	-	2.0033	0.0077
201653_at	10175	CNIH	cornichon homolog (Drosophila)	2.0187	0.0078
217909_s_at	6945	MLX	MAX-like protein X	2.0074	0.0079
213882_at	83941	TM2D1	TM2 domain containing 1	2.0145	0.0078
238935_at	51065	RPS27L	ribosomal protein S27-like	2.0046	0.0079
202168_at	6880	TAF9	TAF9 RNA polymerase II, TATA box binding protein (TBP)-associated factor, 32kDa	2.0091	0.0083
202829_s_at	6845	VAMP7	vesicle-associated membrane protein 7	2.0062	0.0084
203300_x_at	8905	AP1S2	adaptor-related protein complex 1, sigma 2 subunit	2.0004	0.0083
208905_at	54205	CYCS	cytochrome c, somatic	2.0106	0.0085

Epilogue

Although the hallmarks of cancer seem to be unified among all cancer types, regardless of the tissue of origin, there is an enormous heterogeneity not only between different tumors, but also at the cellular level within a given tumor. The discovery of cancer stem cells has opened a new field of research and the appearance of CSC in various tumor types starts to be considered as a new hallmark of cancer. Despite the fact that CSC from different tumors can be isolated with the same set of cell surface markers, it seems that there is no unified profile of CSC. As in the case of other cancer hallmarks, like proliferation, the observations from different cancer cell types point to the same functional phenotype that can be however underlined by an array of biological alterations. Thus, understanding the details of molecular biology governing CSC in different tumor types would be crucial for finding new therapeutic solutions to eliminate those cells.

Cancer stem cells can be isolated with cell surface markers, of often uncertain significance for the cellular biology. However, "stemness" of a given cancer cell can be determined only functionally, in spherogenic, tumorigenic and differentiation assays. Thus, finding specific CSC markers that could also serve as therapeutic targets requires careful investigation of their role in those cells. In this work a new function of well-described CSC marker CD44 has been found. Although nuclear localization of the full-length CD44 and its role in transcription does not seem to be dependent on cell tumorigenicity, it could well be that this function is also important for the CSC. Therefore, a new feature of multifunctional CD44 presented in this study might help to establish why many CSC from different tumors express this protein.

The second part of the present work resulted in identification of new biological feature of CSC. The discovery of Imp2 as a regulator of OxPhos in CSC has shed new light on metabolism of those cells. OxPhos dependence of CSC underlines another important functional difference between those cells and the bulk of a tumor and at the same time couples them to normal stem cells, which also use OxPhos as the major energy producing pathway. This new metabolic difference between CSC and their more differentiated counterparts can lead to identification of novel markers or therapeutical targets.

Summarizing, the two projects described in this work present two different approaches – a study of a well known CSC marker to uncover its new functions and

an attempt to find a new function for a protein highly expressed by CSC. Both types of investigation can help to gather new data crucial for understanding the biology of CSC.

Acknowledgements

I would like to thank Professor Ivan Stamenkovic for allowing me to do my thesis in his laboratory, with a great balance between scientific freedom and guidance, and for giving me the opportunity to work in the cancer stem cell field.

I would like to thank Mario Suva, who was constantly involved in the Imp2 project (despite the time zone difference), for his continuous support and motivation and lots of new ideas, particularly the ones sent by sms…

Many thanks to Claudio De Vito for many discussions on the experiments, sharing the bench and some buffers…

Many thanks also to Nicolo Riggi for his long list of ideas and for the support.

I am very grateful to Carlo Fusco, Luisa Cironi and Marina Bacac for creating the core of the lab and sharing the experimental experience.

I thank my collegues Karine Baumer, Marie-Aude Le Bitoux, Sandrine Cornaz, Cynthia Dayer, Tanja Petricevic, Anne Planche for always being ready to help and for the cheerful atmosphere in the lab. And to Phil Shaw for making it even more cheerful. Special thanks to Marie-Aude, Sandrine and Anne for their help with the French version of the thesis summary.

I would also like to thank my parents for all the support and advice.

Finally, I would like to thank Robert for his patience, taking care of all the things I was not and for all those hours of great scientific discussions.

References

1. Hanahan, D. and Robert A. Weinberg, *Hallmarks of Cancer: The Next Generation.* Cell, 2011. **144**(5): p. 646-674.
2. Welte, Y., et al., *Cancer stem cells in solid tumors: elusive or illusive?* Cell Communication and Signaling, 2010. **8**(1): p. 6.
3. Dick, J.E., *Stem cell concepts renew cancer research.* Blood, 2008. **112**(13): p. 4793-4807.
4. Dick, J.E., *Normal and leukemic human stem cells assayed in SCID mice.* Seminars in Immunology, 1996. **8**(4): p. 197-206.
5. Bonnet, D. and J.E. Dick, *Human acute myeloid leukemia is organized as a hierarchy that originates from a primitive hematopoietic cell.* Nature Medicine, 1997. **3**(7): p. 730-737.
6. Singh, S.K., et al., *Identification of human brain tumour initiating cells.* Nature, 2004. **432**(7015): p. 396-401.
7. Al-Hajj, M., et al., *Prospective identification of tumorigenic breast cancer cells.* Proceedings of the National Academy of Sciences, 2003. **100**(7): p. 3983-3988.
8. Ricci-Vitiani, L., et al., *Identification and expansion of human colon-cancer-initiating cells.* Nature, 2007. **445**(7123): p. 111-115.
9. O/'Brien, C.A., et al., *A human colon cancer cell capable of initiating tumour growth in immunodeficient mice.* Nature, 2007. **445**(7123): p. 106-110.
10. Ailles, L.E. and I.L. Weissman, *Cancer stem cells in solid tumors.* Current Opinion in Biotechnology, 2007. **18**(5): p. 460-466.
11. Zöller, M., *CD44: can a cancer-initiating cell profit from an abundantly expressed molecule?* Nat Rev Cancer, 2011. **11**(4): p. 254-267.
12. Collins, A.T., et al., *Prospective Identification of Tumorigenic Prostate Cancer Stem Cells.* Cancer Research, 2005. **65**(23): p. 10946-10951.
13. Zhang, S., et al., *Identification and Characterization of Ovarian Cancer-Initiating Cells from Primary Human Tumors.* Cancer Research, 2008. **68**(11): p. 4311-4320.
14. Griguer, C.E., et al., *CD133 Is a Marker of Bioenergetic Stress in Human Glioma.* PLoS ONE, 2008. **3**(11): p. e3655.
15. Visvader, J.E., *Cells of origin in cancer.* Nature, 2011. **469**(7330): p. 314-322.
16. Hirschmann-Jax, C., et al., *A distinct "side population" of cells with high drug efflux capacity in human tumor cells.* Proceedings of the National Academy of Sciences of the United States of America, 2004. **101**(39): p. 14228-14233.
17. Burkert, J., W.R. Otto, and N.A. Wright, *Side populations of gastrointestinal cancers are not enriched in stem cells.* The Journal of Pathology, 2008. **214**(5): p. 564-573.
18. Lichtenauer, U.D., et al., *Side Population Does Not Define Stem Cell-Like Cancer Cells in the Adrenocortical Carcinoma Cell Line NCI h295R.* Endocrinology, 2008. **149**(3): p. 1314-1322.
19. Platet, N., et al., *Fluctuation of the SP/non-SP phenotype in the C6 glioma cell line.* FEBS Letters, 2007. **581**(7): p. 1435-1440.

20. Aruffo, A., et al., *CD44 is the principal cell surface receptor for hyaluronate.* Cell, 1990. **61**(7): p. 1303-1313.
21. Mackay, C.R., et al., *Expression and Modulation of CD44 Variant Isoforms in Humans.* The Journal of Cell Biology, 1994. **124**(1/2): p. 71-82.
22. Naor, D., et al., *Involvement of CD44, a molecule with a thousand faces, in cancer dissemination.* Seminars in Cancer Biology, 2008. **18**(4): p. 260-267.
23. Ponta, H., L. Sherman, and P.A. Herrlich, *CD44: From adhesion molecules to signalling regulators.* Nat Rev Mol Cell Biol, 2003. **4**(1): p. 33-45.
24. Thorne, R.F., J.W. Legg, and C.M. Isacke, *The role of the CD44 transmembrane and cytoplasmic domains in co-ordinating adhesive and signalling events.* Journal of Cell Science, 2004. **117**(3): p. 373-380.
25. Qin Yu, I.S., *Cell surface-localized matrix metalloproteinase-9 proteolytically activates TGF-β and promotes tumor invasion and angiogenesis.* Genes & Development, 2000. **14**(2): p. 163–176.
26. Yu, W.-H., et al., *CD44 anchors the assembly of matrilysin/MMP-7 with heparin-binding epidermal growth factor precursor and ErbB4 and regulates female reproductive organ remodeling.* Genes & Development, 2002. **16**(3): p. 307-323.
27. Martin, T.A., et al., *The role of the CD44/ezrin complex in cancer metastasis.* Critical Reviews in Oncology/Hematology, 2003. **46**(2): p. 165-186.
28. Xu, Y., I. Stamenkovic, and Q. Yu, *CD44 Attenuates Activation of the Hippo Signaling Pathway and Is a Prime Therapeutic Target for Glioblastoma.* Cancer Research, 2010. **70**(6): p. 2455-2464.
29. Okamoto, I., et al., *Proteolytic release of CD44 intracellular domain and its role in the CD44 signaling pathway.* Journal of Cell Biology, 2001. **155**(5): p. 755-762.
30. Avigdor, A., et al., *CD44 and hyaluronic acid cooperate with SDF-1 in the trafficking of human CD34+ stem/progenitor cells to bone marrow.* Blood, 2004. **103**(8): p. 2981-2989.
31. Liu J, J.G., *CD44 and hematologic malignancies.* Cellular & Molecular Immunology, 2006. **3**(5): p. 359-65.
32. Bourguignon, L.Y.W., et al., *Hyaluronan-CD44 Interaction Activates Stem Cell Marker Nanog, Stat-3-mediated MDR1 Gene Expression, and Ankyrin-regulated Multidrug Efflux in Breast and Ovarian Tumor Cells.* Journal of Biological Chemistry, 2008. **283**(25): p. 17635-17651.
33. Wielenga, V.J.M., et al., *Expression of CD44 in Apc and TcfMutant Mice Implies Regulation by the WNT Pathway.* The American Journal of Pathology, 1999. **154**(2): p. 515-523.
34. Nagano, O. and H. Saya, *Mechanism and biological significance of CD44 cleavage.* Cancer Science, 2004. **95**(12): p. 930-935.
35. Cansizoglu, A.E., et al., *Structure-based design of a pathway-specific nuclear import inhibitor.* Nature Structural & Molecular Biology, 2007. **14**(5): p. 452-454.
36. Lee, B.J., et al., *Rules for nuclear localization sequence recognition by karyopherin beta 2.* Cell, 2006. **126**(3): p. 543-558.
37. Murakami, D., et al., *Presenilin-dependent gamma-secretase activity mediates the intramembranous cleavage of CD44.* Oncogene, 2003. **22**(10): p. 1511-1516.

38. Imasaki, T., et al., *Structural Basis for Substrate Recognition and Dissociation by Human Transportin 1.* Molecular Cell, 2007. **28**(1): p. 57-67.
39. Evanko, S.P. and T.N. Wight, *Intracellular Localization of Hyaluronan in Proliferating Cells.* Journal of Histochemistry & Cytochemistry, 1999. **47**(10): p. 1331-1341.
40. Goley, E.D. and M.D. Welch, *The ARP2/3 complex: an actin nucleator comes of age.* Nat Rev Mol Cell Biol, 2006. **7**(10): p. 713-726.
41. Yoo, Y., X. Wu, and J.-L. Guan, *A Novel Role of the Actin-nucleating Arp2/3 Complex in the Regulation of RNA Polymerase II-dependent Transcription.* Journal of Biological Chemistry, 2007. **282**(10): p. 7616-7623.
42. Roberts, C.W.M. and S.H. Orkin, *The SWI/SNF complex [mdash] chromatin and cancer.* Nat Rev Cancer, 2004. **4**(2): p. 133-142.
43. Strobeck, M.W., et al., *The BRG-1 Subunit of the SWI/SNF Complex Regulates CD44 Expression.* Journal of Biological Chemistry, 2001. **276**(12): p. 9273-9278.
44. Son, M.J., et al., *SSEA-1 Is an Enrichment Marker for Tumor-Initiating Cells in Human Glioblastoma.* Cell stem cell, 2009. **4**(5): p. 440-452.
45. Peñuelas, S., et al., *TGF-[beta] Increases Glioma-Initiating Cell Self-Renewal through the Induction of LIF in Human Glioblastoma.* Cancer cell, 2009. **15**(4): p. 315-327.
46. Louis, D.N., *MOLECULAR PATHOLOGY OF MALIGNANT GLIOMAS.* Annual Review of Pathology: Mechanisms of Disease, 2006. **1**(1): p. 97-117.
47. Adamson, C., et al., *Glioblastoma multiforme: a review of where we have been and where we are going.* Expert Opinion on Investigational Drugs, 2009. **18**(8): p. 1061-1083.
48. Sofroniew, M. and H. Vinters, *Astrocytes: biology and pathology.* Acta Neuropathologica, 2010. **119**(1): p. 7-35.
49. Sanai, N., et al., *Unique astrocyte ribbon in adult human brain contains neural stem cells but lacks chain migration.* Nature, 2004. **427**(6976): p. 740-744.
50. Lobo, N.A., et al., *The Biology of Cancer Stem Cells.* Annual Review of Cell and Developmental Biology, 2007. **23**(1): p. 675-699.
51. Holland, E.C., et al., *Combined activation of Ras and Akt in neural progenitors induces glioblastoma formation in mice.* Nat Genet, 2000. **25**(1): p. 55-57.
52. Uchida, N., et al., *Direct isolation of human central nervous system stem cells.* Proceedings of the National Academy of Sciences, 2000. **97**(26): p. 14720-14725.
53. Yisraeli, J.K., *VICKZ proteins: a multi-talented family of regulatory RNA-binding proteins.* Biol. Cell, 2005. **97**(1): p. 87-96.
54. Christiansen, J., et al., *IGF2 mRNA-binding protein 2: biological function and putative role in type 2 diabetes.* J Mol Endocrinol, 2009. **43**(5): p. 187-195.
55. Yaniv, K. and J.K. Yisraeli, *The involvement of a conserved family of RNA binding proteins in embryonic development and carcinogenesis.* Gene, 2002. **287**(1-2): p. 49-54.
56. Boudoukha, S., S. Cuvellier, and A. Polesskaya, *Role of the RNA-Binding Protein IMP-2 in Muscle Cell Motility.* Mol. Cell. Biol., 2010. **30**(24): p. 5710-5725.

57. Adolph, S.K., et al., *Embryonic expression of Drosophila IMP in the developing CNS and PNS.* Gene Expression Patterns, 2009. **9**(3): p. 138-143.
58. Vander Heiden, M.G., L.C. Cantley, and C.B. Thompson, *Understanding the Warburg Effect: The Metabolic Requirements of Cell Proliferation.* Science, 2009. **324**(5930): p. 1029-1033.
59. Sun, L., et al., *Neuronal and glioma-derived stem cell factor induces angiogenesis within the brain.* Cancer cell, 2006. **9**(4): p. 287-300.
60. Moreno-Sánchez, R., et al., *Energy metabolism in tumor cells.* FEBS Journal, 2007. **274**(6): p. 1393-1418.
61. Jose, C., N. Bellance, and R. Rossignol, *Choosing between glycolysis and oxidative phosphorylation: A tumor's dilemma?* Biochimica et Biophysica Acta (BBA) - Bioenergetics, 2011. **1807**(6): p. 552-561.
62. Plotnikov EY, M.M., Podgornyi OV, Aleksandrova MA, Zorov DB, Sukhikh GT., *Functional activity of mitochondria in cultured neural precursor cells.* Cell Technologies in Biology and Medicine, 2006. **2**(1): p. 142-146.
63. Lonergan, T., C. Brenner, and B. Bavister, *Differentiation-related changes in mitochondrial properties as indicators of stem cell competence.* Journal of Cellular Physiology, 2006. **208**(1): p. 149-153.
64. Schieke, S.M., et al., *Mitochondrial Metabolism Modulates Differentiation and Teratoma Formation Capacity in Mouse Embryonic Stem Cells.* Journal of Biological Chemistry, 2008. **283**(42): p. 28506-28512.
65. Funes, J.M., et al., *Transformation of human mesenchymal stem cells increases their dependency on oxidative phosphorylation for energy production.* Proceedings of the National Academy of Sciences, 2007. **104**(15): p. 6223-6228.
66. Borovski, T., et al., *Cancer Stem Cell Niche: The Place to Be.* Cancer Research, 2011. **71**(3): p. 634-639.
67. Calabrese, C., et al., *A Perivascular Niche for Brain Tumor Stem Cells.* Cancer cell, 2007. **11**(1): p. 69-82.
68. Ricci-Vitiani, L., et al., *Tumour vascularization via endothelial differentiation of glioblastoma stem-like cells.* Nature, 2010. **468**(7325): p. 824-828.
69. Lathia, Justin D., et al., *Deadly Teamwork: Neural Cancer Stem Cells and the Tumor Microenvironment.* Cell stem cell, 2011. **8**(5): p. 482-485.
70. Wallace, D.C., *A MITOCHONDRIAL PARADIGM OF METABOLIC AND DEGENERATIVE DISEASES, AGING, AND CANCER: A Dawn for Evolutionary Medicine.* Annual Review of Genetics, 2005. **39**(1): p. 359-407.
71. Verner, K., *Co-translational protein import into mitochondria: an alternative view.* Trends in Biochemical Sciences, 1993. **18**(10): p. 366-371.
72. Hammer, N.A., et al., *Expression of IGF-II mRNA-binding proteins (IMPs) in gonads and testicular cancer.* Reproduction, 2005. **130**(2): p. 203-212.
73. Dai, N., et al., *mTOR phosphorylates IMP2 to promote IGF2 mRNA translation by internal ribosomal entry.* Genes & Development, 2011.